



universität
wien

DIPLOMARBEIT

Titel der Diplomarbeit

Spectroscopy of nanopore water

angestrebter akademischer Grad

Magister der Naturwissenschaften (Mag. rer. nat.)

Verfasser:	Marcus Weinwurm
Matrikel-Nummer:	0503370
Studienrichtung:	411 Physik
Betreuer:	Univ.-Prof. Dr. Christoph Dellago

Wien, am 10. Juni 2010

Danksagung

Bis zum Abschluss eines Physikstudiums ist es ein langer Weg auf dem man von vielen Menschen begleitet und unterstützt wird. Von Geburt an ist man auf seine Eltern angewiesen, welche anfangs das Steuer übernehmen und einem dann später immer mehr Freiheiten in die Hand geben, um seine Persönlichkeit zu entfalten. Ich kann mich glücklich schätzen, dass meine Mutter und mein Vater schon sehr bald auf meine Entscheidungsfähigkeit vertraut haben und mir bei der Verwirklichung meiner Ziele und Vorstellungen immer ohne Bedingungen geholfen haben und auch weiterhin helfen. Sie gaben Geborgenheit innerhalb einer Familie, wertvolle Ratschläge in schwierigen Zeiten und auch finanzielle Absicherung. Zu Ersterem haben natürlich auch meine beiden Schwestern mitgewirkt, die das gemeinsame Zusammenleben immer lebhaft gestalteten. Weiters hat meine Großmutter Ihren Teil dazu beigetragen, indem Sie mich stets liebevoll kulinarisch versorgte und Ihr Ersparnis gern in mich investierte.

Unerlässlich sind aber auch Freunde, mit denen man Erfahrungen teilt und die das gemeinsame Schulbankdrücken auflockerten. Mit vielen von ihnen, die ich schon seit der Hauptschule, Volksschule oder sogar dem Kindergarten kenne, bin ich jetzt noch befreundet, und lerne von ihnen jene Dinge, die nicht in Büchern stehen.

Wichtig waren auch die Mitglieder meiner Arbeitsgruppe, die mir beim Verfassen meiner Diplomarbeit stets mit Rat und Tat zur Seite standen, und auch abseits des universitären Alltags zu guten Freunden wurden.

Zu guter Letzt hat mir Christoph Dellago mit dem Betreuen dieser Diplomarbeit, seinen stets kreativen Ideen und seiner wissenschaftlichen Erfahrung einen Einstieg in die universitäre Forschung ermöglicht, wie man ihn sich besser wohl nicht vorstellen könnte.

Hiermit möchte ich allen danken die mir auf meinem Weg geholfen haben!

Abstract

We study vibrational spectra of water confined inside various types of carbon nanotubes. The water molecules form different kinds of ordered structures depending on temperature, density and the diameter of the nanopore. We simulate the system using molecular dynamics methods and apply perturbation theory to calculate vibrational frequencies. We study the motional narrowing effect in these systems by taking into account the vibrational lifetime of OH excitations and the dipole-dipole time correlation of the OH stretch. The resulting spectra reveal the distinct order in the different tubes, and suggest that these structures can also be tested experimentally through infrared spectroscopy. Furthermore, we compare the strong correlation between the E-field at the hydrogen and the vibrational frequency in these systems to the correlation in bulk.

Zusammenfassung

In dieser Arbeit behandeln wir mit Wasser gefüllte Kohlenstoffnanoröhren und deren Vibrationsspektren. Unter diesem zylindrischen Einschluss bilden sich vielfältige geordnete Strukturen je nach Dichte und Temperatur des Wassers und Durchmesser der Röhren. Wir simulieren die Systeme unter Anwendung von Molekulardynamikmethoden und wenden Störungsrechnung an, um Vibrationsfrequenzen zu berechnen. Wir untersuchen auch den Effekt der Linienverschmälerung indem wir die Lebensdauer eines angeregten OH Zustandes und die Dipol-Dipol-Korrelationen der OH Bindung berücksichtigen. Die resultierenden Spektren lassen sich eindeutig verschiedenen Konfigurationen des Systems zuordnen und legen nahe, dass diese Wasserstrukturen auch experimentell mittels Infrarotspektroskopie getestet werden könnten. Weiters vergleichen wir die starke Korrelation zwischen dem E-Feld am Wasserstoff und der Vibrationsfrequenz in diesen Systemen zur Korrelation in der ausgedehnten Flüssigkeit.

Contents

1	Introduction	1
2	Models	3
2.1	1D Ising model	3
2.2	Water chains of finite size	4
2.3	SPC/E	5
2.4	Carbon nanotube	6
2.5	OH vibration	8
3	Methods	13
3.1	Molecular dynamics	13
3.1.1	Verlet algorithm	13
3.1.2	SHAKE algorithm	14
3.1.3	1D lattice sums	15
3.2	Spectroscopy	17
3.2.1	Infrared spectroscopy	17
3.2.2	Raman spectroscopy	17
3.2.3	Optical absorption coefficient	18
3.2.4	Calculating IR absorption spectra	20
3.3	Time correlation functions	20
4	Numerical results	23
4.1	Simulation details	23
4.2	Dipole-dipole time correlation function	24
4.3	Oxygen-oxygen and hydrogen-hydrogen radial distribution functions	25
4.4	OH angle pair distribution functions	27

4.5	E-field distributions	29
4.6	Frequency distribution	31
4.7	E_H - ω_{OH} correlation	32
4.8	E_H - G correlation	34
4.9	Temperature dependence	35
4.10	Infrared spectrum	36
4.11	Wide carbon nanotubes	37
4.11.1	Structure	38
4.11.2	Frequency distributions and spectra	40
4.12	Water dimer	43
5	Final remarks	47
A	Derivation of the eigenfunctions	
	of the Schrödinger equation for the Morse potential	49

Chapter 1

Introduction

In previous works, it was shown that at ambient conditions single walled carbon nanotubes tubes fill with water, even in tubes with diameters around 0.8 nm [1]. Other studies confirmed water filling through Raman spectroscopy [2], and recent experiments by Cambre, Schoeters, Luyckx, Goovaerts and Wenseleers confirmed filling down to chiral index (5,3) [3].

Water confined in narrow carbon nanotubes turned out to have many intriguing properties. In tubes with diameters around 0.8 nm water forms a single file chain, where the molecules are linked together through hydrogen bonds. Köfinger, Dellago and Hummer showed that it is possible to describe such chains with a dipole lattice model and found nearly perfect dipolar order for tube lengths up to 0.1 mm [4]. Köfinger and Dellago also suggested experimental procedures to probe the ordering [5]. Another interesting phenomenon is the flow of water through such tubes. It turns out that the flow rates are considerably higher than estimated by continuum hydrodynamics. Furthermore, Dellago, Naor and Hummer found that proton transport in single-file water is up to 40 times faster compared to bulk water [6]. Membranes of carbon nanotubes can be viewed as model systems for biological membranes, and proton transport in these systems was also studied [7]. In tubes larger than 1 nm the water molecules form cylindrical structures [8]. The phase diagram of such systems was studied and even double and triple layered water cylinders were found for tubes wider than 1.5 nm [9].

In this work we study the electromagnetic absorption spectrum of single-file water in a (6,6) carbon nanotube and water structures in wider tubes.

In the first case, each water molecule is situated in a chain, shares one hydrogen bond and accepts another one from its neighbours. One of the hydrogen atoms is free, without any hydrogen bonding, the other one is bonded. Due to this separation into two types of hydrogens, the overall electric field distribution at the hydrogens has two major contributions. Since the E-fields at the hydrogen influence the OH vibrational frequency significantly, we expect two well separated peaks in the spectrum. This effect should even be more pronounced in the infrared spectrum compared to the Raman spectrum, due to motional narrowing.

In the past there were several works on the OH stretch frequency ω_{OH} in water. Nakamoto, Margoshes and Rundle described the relationship between hydrogen bonding distances and ω_{OH} [10]. Novak showed the strong correlation between the intermolecular oxygen-oxygen distance and ω_{OH} [11]. Time-resolved transient hole burning has been used to study structural dynamics in glasses. Several computational works on nonlinear infrared spectroscopy described vibrational dephasing in HOD in D₂O. Eaves, Tokmakoff and Geissler found a very strong linear correlation between the electric field at the hydrogen and ω_{OH} [12]. Corcelli and Skinner calculated the temperature dependence of infrared and Raman line shapes of HOD in H₂O and D₂O [13]. Reischl, Köfinger, Dellago and Hummer described the shell contributions of surrounding water molecules to the electric field in the middle of the OH bond [14].

Chapter 2

Models

2.1 1D Ising model

Before we describe single file water theoretically, we first would like to remind the reader of a fundamental model system of statistical physics. The one-dimensional Ising model is closely related to single-file water chains, which are in the focus of our interest. The 1D Ising Model consists of dipole moments aligned in an infinitely long chain. Each dipole moment D_i interacts only with its nearest neighbours and can only take the values -1 or $+1$. The Hamiltonian H takes the form:

$$H = -J \sum_i D_i D_{i+1} . \quad (2.1)$$

For $J > 0$, it is favorable for the dipoles to align in the same direction, and we would expect that for low temperatures the system goes into an ordered phase, which involves a net magnetization. But surprisingly, this model does not show a phase transition. Order takes place only at $T = 0$, where the entropic terms vanish. We explain this by use of an expression for the free energy F :

$$F = H - T S . \quad (2.2)$$

Here H is the energy, T is the temperature and S is the entropy. A stable configuration of the system has to be a minimum of the free energy. Let us imagine an ordered chain where all dipoles are aligned and an unordered chain where the dipoles left of the center are -1 and the others are $+1$. In

the latter, the energy cost of the defect at the center is little compared to the gain in entropy. The entropic term $T S$ lowers the free energy for states with high entropy (disorder) and thus the system is always in a disordered state except for $T = 0$. However, in two dimensions the energy cost of a defect is much higher and the system goes into an ordered phase below a certain temperature T_c . [15].

2.2 Water chains of finite size

Since water has a dipole moment, it is possible to describe the properties of water confined in narrow nanotubes by using a dipole lattice model similar to the 1D Ising. The difference is that the dipoles σ_j can take the values (1,-1,0) and every dipole i interacts with every other j via a $1/r^3$ potential ϕ_{ij} .

$$\phi_{ij} = -\frac{\varepsilon \sigma_i \sigma_j}{|i - j|^3} \quad (2.3)$$

Köfinger, Dellago and Hummer showed that this model describes the main properties of this system sufficient and parameterized it against molecular dynamics simulations [4].

These studies also showed that the contact energy between next neighbour dipoles is different from the dipole-dipole interaction energy such that the Hamiltonian takes the form:

$$H = \sum_{\beta=1}^{N-1} \sum_{\alpha=\beta+1}^N \phi_{ij} + (n - n_c)(1 + E_c) - 2n_d + n_c S_c. \quad (2.4)$$

Here, we added the contact energy E_c of the $(n - n_c)$ parallel oriented neighbours, subtracted the dipole interaction for $(n - n_c - 2n_d)$ next neighbour pairs of parallel dipoles and added an entropic contribution S_c for the end of ordered segments. The entropic contribution takes into account that water molecules at the end of ordered chains have a larger set of possible configurations available to them.

Köfinger, Dellago and Hummer found that such water chains are ordered at room temperature up to lengths of 10^5 molecules [4]. This corresponds to a tube length of 0.05 mm. Occasionally, pairs of oriental defects arise,

see Fig. 2.2, but they do not destroy the global order. Note that this does not contradict the result for the 1D Ising model, since the water chains are of finite size. For tubes longer than 1 mm the chains are disordered as suggested by the Ising model.

2.3 SPC/E

To simulate water we use the SPC/E model invented by Berendsen, Grigera and Straatsma [16]. In this model, each water molecule carries an oxygen charge of $-0.8476e$ and an hydrogen charge of $0.4238e$. The water molecules are rigid with an HOH angle of 109.47° and an OH bond length of 1 \AA . A Lennard Jones center is located at the oxygen site with parameters $A = 629400 \text{ kcal/mol \AA}^{12}$ and $B = 625.5 \text{ kcal/mol \AA}^6$.

Since the model is rigid, vibrational couplings and vibrational energy transfer are neglected. In particular, we simulate HOD in D_2O and the coupling of OH oscillators is inhibited.

The model also does not feature changes in electron density induced by surrounding molecules. Although there are several good polarizable water models available, we used the simpler SPC/E model because polarization is expected to have only minor effects in our system.

The behavior of our system depends very much on the hydrogen bonding topology. The SPC/E model describes only the electrostatic character of the hydrogen bond and neglects the covalent character. Since the SPC/E

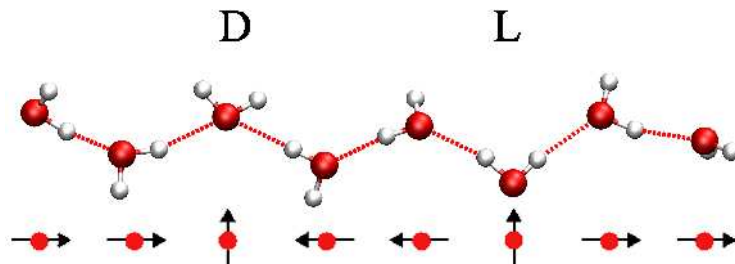


Figure 2.1: Example of a defect configuration in a water chain. In case of the D-defect(L-defect) the molecule accepts (donates) two hydrogen bonds (top). In the dipole picture both defects are represented by dipoles pointing in a direction orthogonal to the tube axis (bottom) [1].

model reproduces the bulk properties of liquid water accurately, we expect that this approximation is suitable for our system.

2.4 Carbon nanotube

To model the carbon nanotube we use a polynomial potential V which interacts with the oxygen atoms:

$$V(r) = a_2 r^2 + a_4 r^4 + a_6 r^6 + a_8 r^8, \quad (2.5)$$

where r is the radial distance from the cylinder axis. The parameters a_n of the potential are

$$\begin{aligned} a_2 &= -0.2281 \text{ kcal/mol } \text{\AA}^{-2} \\ a_4 &= 1.09 \text{ kcal/mol } \text{\AA}^{-4} \\ a_6 &= 0.2341 \text{ kcal/mol } \text{\AA}^{-6} \\ a_8 &= 0.3254 \text{ kcal/mol } \text{\AA}^{-8}, \end{aligned} \quad (2.6)$$

and have been determined by fitting the polynomial in Equ. (2.5) to $-k_B T \ln \rho(r)$, where $\rho(r)$ is the radial density profile of a single water molecule in a (6,6) armchair-type carbon nanotube [6].

To obtain a measure for the volume of this (6,6) carbon nanotube we define the characteristic volume V_c :

$$V_c := \int_V \exp \left(- \frac{V(r)}{k_B T} \right) dv. \quad (2.7)$$

Furthermore, we define the characteristic radius:

$$r_c := \sqrt{\frac{V_c}{\pi}}. \quad (2.8)$$

In Fig. 2.2 the tube potential, the characteristic radius r_c and $k_B T$ are plotted in one frame.

To obtain the confining potential corresponding to wider tubes out of the (6,6) tube potential we make the approximation that the potential for the wider tubes is equal to zero near the tube axis and let the usual (6,6)

potential start at the radius difference between the wider tube and the (6,6) tube.

$$V(r) = 0 \text{ for } 0 < r < (d_n - d_{6,6})/2. \quad (2.9)$$

$$V(r) = a_2(r - r_{n^*})^2 + a_4(r - r_{n^*})^4 + a_6(r - r_{n^*})^6 + a_8(r - r_{n^*})^8 \quad (2.10)$$

for $r > (d_n - d_{6,6})/2 = r_{n^*}$

We used the following diameters d_n of different single walled carbon nanotubes in our simulations:

- (6,6) $d_{6,6} = 0.81 \text{ nm}$
- (8,8) $d_{8,8} = 1.09 \text{ nm}$
- (9,8) $d_{9,8} = 1.15 \text{ nm}$
- (9,9) $d_{9,9} = 1.22 \text{ nm}$
- (10,10) $d_{10,10} = 1.36 \text{ nm}$

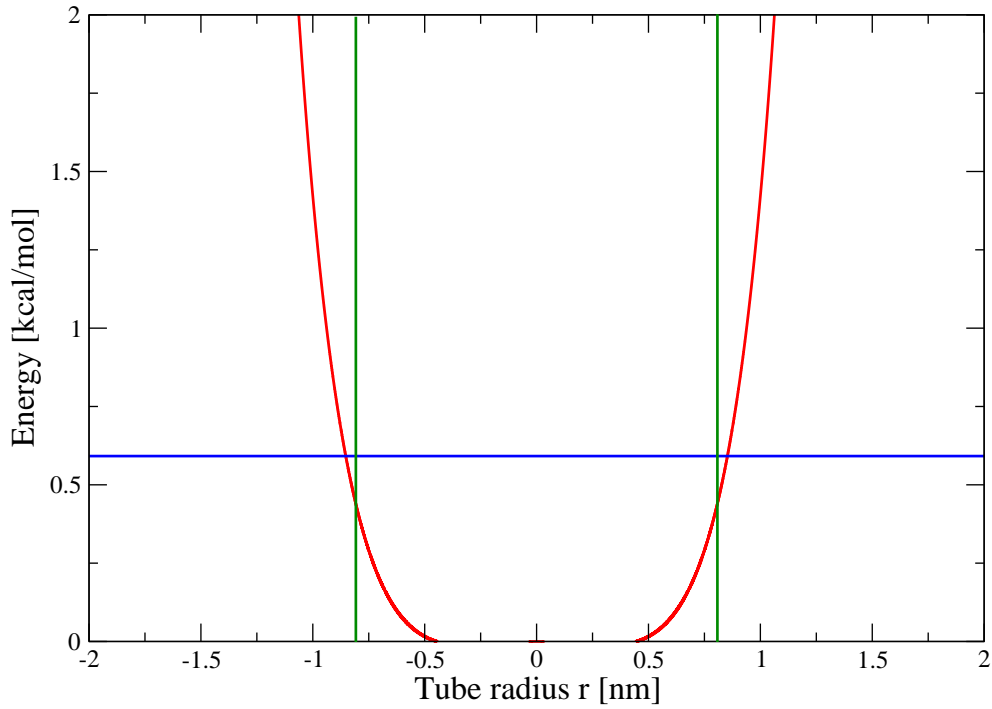


Figure 2.2: red: tube potential energy, blue: $k_B T$, green: r_c

2.5 OH vibration

To describe the OH vibrational frequency of a water molecule we quantize and perturb a 1D Morse oscillator following the derivation of Eaves, Tokmakoff and Geissler [12]. In the past, approaches with quartic potentials were also tried [17]. However, a Morse potential is clearly the best choice for water, because a polynomial potential would be too hard for large distances, see Fig. 2.3. Note that a proton can also dissociate away from the water molecule, which is described by the finite number of energy levels of this model [6]. But that does not mean that we simulate dissociation process, since we are doing a classical simulation with rigid molecules. Nonetheless, the finite energy of the Morse potential's eigenfunctions influences the calculated frequencies.

We neglect intramolecular kinetic coupling to the OD-bond, bending and rotation motion, which are small compared to the intermolecular coupling to the electrostatic interaction [18].

Since the system we study is HOD in D₂O the OH vibration does not

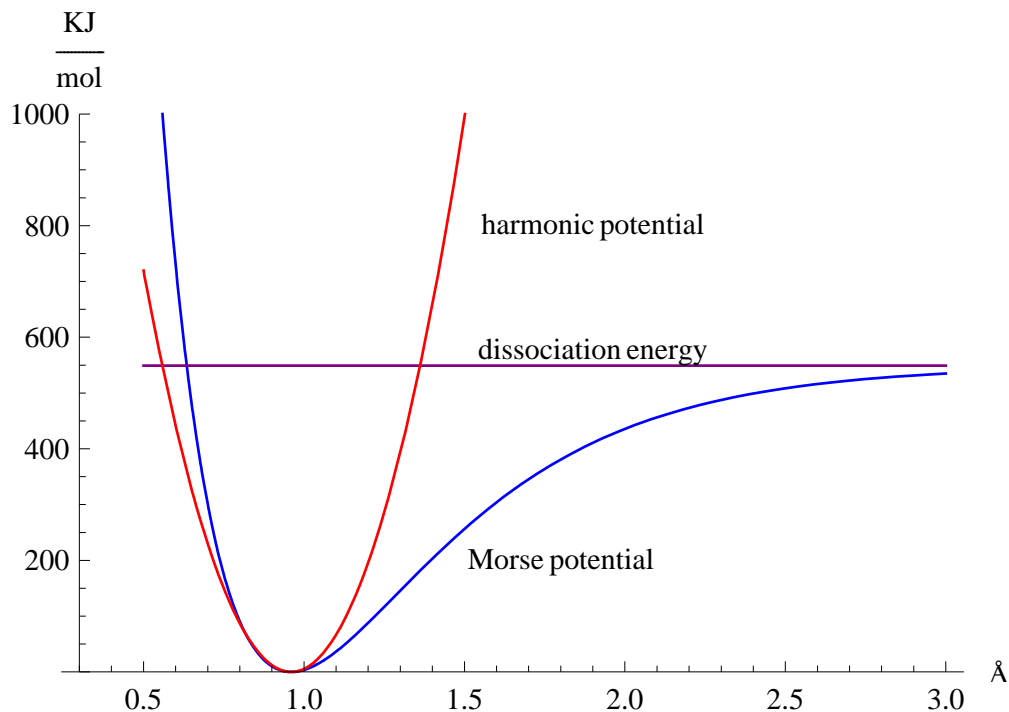


Figure 2.3: Morse potential(blue), harmonic potential(red) and dissociation energy(purple)

couple to other nearby OH oscillators of other molecules. In contrast to H₂O where the OH vibrations are strongly influenced by other nearby OH oscillators in the bath. This simplifies the quantum mechanical part of the Hamiltonian and reduces it to one dimension.

The Hamiltonian H is split into three parts. $H_s(P, Q)$ represents the quantum mechanical vibration of the OH bond with the quantum mechanical degrees of freedom P, Q . $H_b(p, q)$ is the Hamiltonian for the classical bath with the classical degrees of freedom p, q . H_{sb} couples the classical motions of the bath to the quantum mechanical vibration. The full Hamiltonian takes the form:

$$H = H_s(P, Q) + H_{sb}(p, q, P, Q) + H_b(p, q) . \quad (2.11)$$

Now we are going to define these three separated Hamiltonians:

H_s is the bare one-dimensional quantum mechanical Morse Oscillator.

$$H_s(P, Q) = \frac{P^2}{2\mu} + d(1 - \exp(-aQ))^2 \quad (2.12)$$

Here, P is the momentum operator, μ is the reduced mass of the oxygen and the hydrogen atom, Q is the internal space coordinate of the vibration, and a, d are parameters of the Morse potential. We express the eigenfunctions $|n\rangle$ of the Schrödinger equation in terms of Laguerre polynomials [19]:

$$|n\rangle = e^{K \exp(-aQ)} [2K \exp(-aQ)]^{K-n-1/2} L_n^{2K-2n-1}(2K \exp[-aQ]) , \quad (2.13)$$

where

$$K = (2\mu d)^{1/2} / a\hbar . \quad (2.14)$$

A derivation can be found in Appendix A. For the potential we used parameters from Reimers and Watts [18]:

$$d = 549.0586 \text{ kJ/mol} ,$$

$$a = 2.13498 \text{ \AA}^{-1} .$$

As you can see in Fig. 2.4 the wave functions Ψ_0 and Ψ_1 are nearly odd or even around the minimum of the potential. Wave functions of higher energy-eigenvalue are influenced by the characteristic shape of the Morse

potential. Ψ_5 is already clearly asymmetric because of the asymmetric potential.

H_{sb} is the interaction between the OH oscillator and the classical bath. To obtain an expression for H_{sb} we calculate the work that the electrostatic field of the surrounding molecules performs on the OH vibration. Note that we are evaluating the forces on the hydrogen and on the oxygen during the classical simulation only at their equilibrium positions. Therefore we have to expand the performed work in internal coordinates. We truncate this expansion at the harmonic level and ignore the momentum terms.

$$H_{sb}(p, q, P, Q) = FQ + GQ^2 \quad (2.15)$$

F and G are derivatives of the Coulomb potential which we are now calculating. To obtain expressions for F and G , we first have to express the derivatives in internal coordinates. The center of mass \vec{r}_c is at the position:

$$\vec{r}_c = \frac{\vec{r}_H m_H + \vec{r}_O m_O}{m_O + m_H} . \quad (2.16)$$

Where r_H and m_H is the position and the mass of the hydrogen and r_O and m_O are the same variables for the oxygen. The internal coordinates \vec{r}_H^* and \vec{r}_O^* in the center of mass frame are:

$$\vec{r}_H^* = \frac{\vec{r}_H m_O - \vec{r}_O m_O}{m_O + m_H} = \frac{(\vec{r}_H - \vec{r}_O) m_O}{m_O + m_H} = \frac{-Q m_O}{m_O + m_H} \quad (2.17)$$

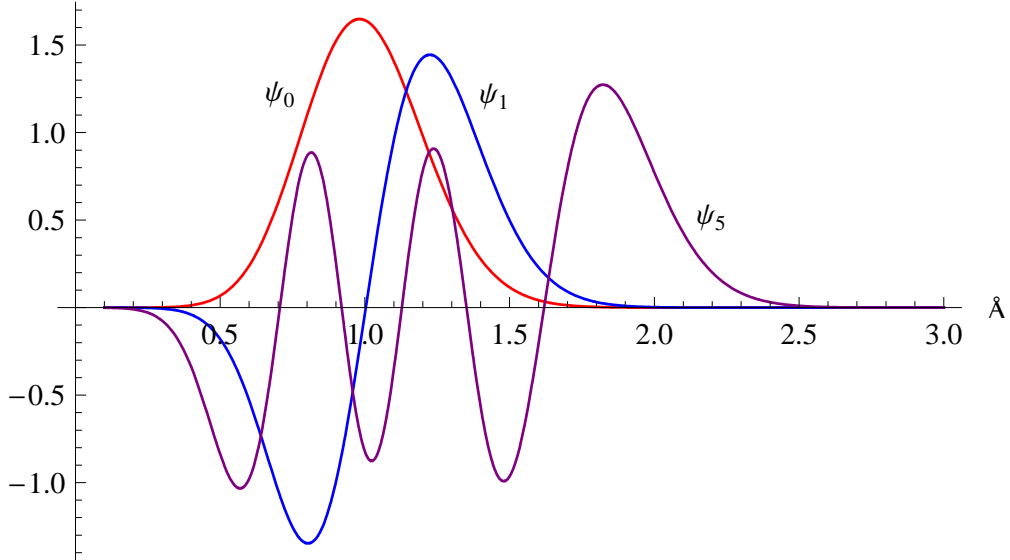


Figure 2.4: Wave functions ψ_0 , ψ_1 , and ψ_5 of the Morse potential

and

$$\vec{r}_O^\dagger = \frac{\vec{r}_H m_H - \vec{r}_O m_H}{m_O + m_H} = \frac{(\vec{r}_H - \vec{r}_O) m_H}{m_O + m_H} = \frac{Q m_H}{m_O + m_H} . \quad (2.18)$$

Since Q is a function of \vec{r}_H^\dagger and \vec{r}_O^\dagger ,

$$Q = Q(\vec{r}_H^\dagger, \vec{r}_O^\dagger) , \quad (2.19)$$

we obtain the expression,

$$\frac{\partial}{\partial Q} = -\mu \hat{r}_{OH} \cdot \left(\frac{\nabla_O}{m_O} - \frac{\nabla_H}{m_H} \right) , \quad (2.20)$$

by applying the chain rule. We apply this operator to the Coulomb potential and obtain:

$$F = \frac{\partial V}{\partial Q} = -\mu \hat{r}_{OH} \cdot \left(\frac{\vec{F}_O}{m_O} - \frac{\vec{F}_H}{m_H} \right) , \quad (2.21)$$

$$G = \frac{\partial^2 V}{\partial Q^2} = \mu^2 \frac{\hat{r}_{OH}^\alpha \hat{r}_{OH}^\beta}{2} \left(\frac{\nabla_O^\alpha \nabla_O^\beta}{m_O^2} - \frac{2 \nabla_O^\alpha \nabla_H^\beta}{m_O m_H} + \frac{\nabla_H^\alpha \nabla_H^\beta}{m_H^2} \right) V . \quad (2.22)$$

We ignore the terms divided by the quadratic mass and half the mass of the oxygen atom and obtain a simplified expression for G :

$$G \approx \mu^2 \hat{r}_{OH}^\alpha \hat{r}_{OH}^\beta \frac{3 r^\alpha r^\beta - r^2 \delta^{\alpha\beta}}{r^5 m_H^2} . \quad (2.23)$$

We used the sum convention for greek indices and hats indicate unit vectors.

Calculating F is obvious, because the forces are available at every time step during a molecular dynamics simulation. G requires additonal computing time, but is feasible with currently available computing power even for large systems.

By having expressions for F and G , we can compute expectation values of vibrational frequencies. We solve the Schrödinger equation for $H_s + H_{sb}$ by use of perturbation theory [20]. H_{sb} shifts the vibrational frequency of the OH bond as a function of the electric field and higher derivatives of the Coulomb potential.

$$(H_s + H_{sb})\Psi[q(t)] = (E_{sn} + E_{sbn})[q(t)]\Psi[q(t)] \quad (2.24)$$

We perturb the solutions $|n\rangle$ of H_s to obtain E_{sbn} :

$$E_{sbn} = \langle n | H_{sb} | n \rangle + \sum_{k, n \neq k} \frac{|\langle n | H_{sb} | k \rangle|^2}{e_n - e_k} . \quad (2.25)$$

The second order term is usually small and first order perturbation theory is sufficient. We split the first order term into two parts and get:

$$E_{sbn} = \langle n | FQ + GQ^2 | n \rangle = F \langle n | Q | n \rangle + G \langle n | Q^2 | n \rangle . \quad (2.26)$$

We calculate only transitions between the first two energy levels, since the probability for other transitions is much smaller [21]. The frequencies ω_{OH} are calculated through:

$$\hbar\omega_{OH} = E_{s1} - E_{s0} + E_{sb1} - E_{sb2} . \quad (2.27)$$

The fact that G is small will result in a linear dependence of ω_{OH} as a function of the electric field at the hydrogen in direction of the OH bond. Eaves, Tokmakoff and Geissler showed this in bulk water by calculating the cross-correlation function of the E-field and the OH frequency [12]. We will compare their result to the correlation in single-file water in Chapter 4.7.

Chapter 3

Methods

3.1 Molecular dynamics

Molecular Dynamics is the method which evolves a system of many particles in time by solving Newton's equations of motions iteratively for a given potential $V(r_1, r_2, \dots, r_i, \dots, r_n)$, where r_i is the position of particle i . The forces F_i are calculated from the potential at every timestep:

$$F_i = \frac{\partial V(r_1, \dots, r_n)}{\partial r_i} . \quad (3.1)$$

Velocities v_i and coordinates x_i are calculated from the relation between the momenta p_i and forces F_i :

$$\frac{dp_i}{dt} = \frac{d(m v_i)}{dt} = \frac{m dv_i}{dt} = \frac{m d^2 x_i}{dt^2} = F_i . \quad (3.2)$$

After the system is equilibrated we perform certain measurements. In doing that, we have to take care that the number of measurements is large enough or else we might only see some configurations of the system, which is likely to visit many very different configurations over a long period of time.

3.1.1 Verlet algorithm

The Verlet Algorithm is a method to integrate Newton's equations of motion of order Δt^4 .

We expand the position vector $\vec{r}(t + \Delta t)$:

$$\vec{r}(t + \Delta t) = \vec{r}(t) + \vec{v}(t)\Delta t + \frac{\vec{a}(t)\Delta t^2}{2} + \frac{\vec{b}(t)\Delta t^3}{6} + \mathcal{O}(\Delta t^4) , \quad (3.3)$$

and the position vector $\vec{r}(t - \Delta t)$:

$$\vec{r}(t - \Delta t) = \vec{r}(t) - \vec{v}(t)\Delta t + \frac{\vec{a}(t)\Delta t^2}{2} - \frac{\vec{b}(t)\Delta t^3}{6} + \mathcal{O}(\Delta t^4). \quad (3.4)$$

Where $\vec{a} = d^2\vec{r}(t)/dt^2$ is the acceleration and $\vec{b} = d^3\vec{r}(t)/dt^3$ is the jerk vector.

If we add these two expressions we get:

$$\vec{r}(t + \Delta t) = 2\vec{r}(t) - \vec{r}(t - \Delta t) + \frac{\vec{F}}{m}\Delta t^2 + \mathcal{O}(\Delta t^4). \quad (3.5)$$

By use of the above equation we are able to calculate the new positions $\vec{r}(t + \Delta t)$, if we insert the old positions $\vec{r}(t)$ and the forces $\vec{F}(t)$ at time t . At the next time step we get the positions $\vec{r}(t + 2\Delta t)$ by calculating the forces $\vec{F}(t + \Delta t)$ and again inserting them together with the positions $\vec{r}(t + \Delta t)$ in Equ. (3.5). By iterating this procedure we evolve the system in time. We chose the time step Δt small enough to achieve sufficient energy conservation.

3.1.2 SHAKE algorithm

To simulate water we need a model like SPC/E described above. Water models usually consist of three to six interaction centers. If one evolves a system of such molecules, one has to take care that the distances between these centers remain constant, during the time evolution.

One of the easiest ways to do this is the SHAKE algorithm. This algorithm calculates virtual forces which keep the bond lengths rigid. The important condition for the expressions of these forces is that they do not perform work on the system. Let us look at the two basic equations required to implement this algorithm. With the index i we denote the sites in the water model. For SPC/E these are three. With the index j we denote the neighbour sites within the same molecule. For SPC/E water, every site has two neighbour sites with rigid distances. d_{ij} is the distance between site i and j . d_{ij}^c is the desired distance between site i and j , which remains constant during the whole simulation. The m_i are the masses of the sites. $\vec{r}_{i,j}$ is the vector from site i to site j . l_{ij} scales the force of site i in direction of site j . For i equals j the scaling factor l_{ij} is zero. The other l_{ij} are calculated by

this formula:

$$l_{ij} = \frac{(d_{ij}(t + \Delta t))^2 - d_{ij}^c + O(\Delta t^4)}{2\Delta t^2(m_i^{-1} + m_j^{-1})r_{i,j}(t) \cdot d_{i,j}(t + \Delta t)} . \quad (3.6)$$

$\vec{r}_{i,a}$ is the position vector of interaction site i . $\vec{r}_{i,n}$ is the new position vector, which we calculate by use of the following formula:

$$\vec{r}_{i,n}(t + \Delta t) = \vec{r}_{i,a}(t + \Delta t) + \sum_j \frac{(\Delta t)^2}{m_i} l_{ij}(t) d_{ij}(t) . \quad (3.7)$$

These two steps are approximations and to keep the bonds rigid they have to be iterated in every timestep until the bond lengths are within a certain window. Usually less than three iterations are sufficient to keep the bond length error within 10^{-8} times the desired bond length d_{ij}^c and the constraints do not have an influence on the energy conservation.

3.1.3 1D lattice sums

Very often, computational physicists are interested in investigating infinite systems with long range interactions. It is obvious that this is not manageable on a computer but a common approach in the three-dimensional case to get approximately correct dynamics of such a system is the Ewald summation [22]. This method formally replicates a finite system infinitely often and approximates the sum of interactions of this formally infinite system. Part of this sum is done in Fourier space because it converges there much faster. Although this method produces approximately the right forces for the replicated system, it is not possible to make statements about the phase behaviour of the system due to entropic terms in the free energy. The Ewald sum cannot account for this entropic terms because the size of the system and the number of possibilities for the system to arrange in a certain way are important for the entropy.

To study an infinitely long tube we formally replicate a finite tube along the tube axis and approximate the resulting interaction. Hummer derived an expression for this 1D lattice sum in an unpublished study, which is an analogon to the 3D Ewald sum. We will follow his derivation now.

We begin with a lattice sum of two particles in a box of the length L , a positive charge in the origin and a negative one at (r, z) in cylinder

coordinates. V is the potential of the system and with n we denote the mirror boxes. The potential for the two particles replicated infinitely in both directions is given by:

$$V = -\frac{1}{(r^2 + z^2)^{1/2}} + \sum_{n=1}^{\infty} \left[\frac{2}{nL} - \frac{1}{(r^2 + (nL + z)^2)^{1/2}} - \frac{1}{(r^2 + (nL - z)^2)^{1/2}} \right]. \quad (3.8)$$

The first term is the potential of the particles in the simulation box. The first term in the sum is the potential from the interaction of each particle with his own periodic images, the other two terms describe the interaction of the periodic images between different charges.

To simplify this equation we need the Poisson summation formula:

$$\sum_{n=-\infty}^{\infty} f(t + nT) = \frac{1}{T} \sum_{k=-\infty}^{\infty} F\left(\frac{k}{T}\right) \exp(2\pi i k t / T). \quad (3.9)$$

The left hand side is a sum over the function f which is periodic with period T . $F(\frac{k}{T})$ is the Fourier transform of $f(t + nT)$. We can apply this formula to our problem and calculate the sum in Fourier space as suggested by the formula. With the use of symbolic algebra software we obtain:

$$V = -\frac{4}{L} \sum_{n=1}^{\infty} \cos\left(\frac{2\pi n z}{L}\right) K_0\left(\frac{2\pi n r}{L}\right) + \frac{2}{L} \ln\left(\frac{r}{2L}\right) + \frac{2\gamma}{L}. \quad (3.10)$$

Here, γ is the Euler-Mascheroni constant and K_0 is the Bessel function of the second kind. This sum converges slowly for $r=0$. To improve the convergence we expand Equ. (3.10) in r and obtain:

$$V = \frac{2\gamma}{L} - \frac{1}{(r_{ij}^2 + z_{ij}^2)^{1/2}} + \sum_{k=0}^{\infty} \frac{(-1)^k r_{ij}^{2k}}{L^{2k+1} (2k!!)^2} \left\{ \Upsilon_{2k}\left(1 + \frac{z_{ij}}{L}\right) + \Upsilon_{2k}\left(1 - \frac{z_{ij}}{L}\right) \right\}. \quad (3.11)$$

The $\Upsilon_n(z)$ are the polygamma functions, defined as derivatives of the logarithm of the gamma function:

$$\Upsilon_n(z) = \frac{d^{n+1}}{dx^{n+1}} \ln(\Gamma(z)). \quad (3.12)$$

If we repeat these steps with a generalized expression of the potential containing many particles, we have to sum over all interactions between every

particle pair (ij) and obtain:

$$V = \frac{\gamma}{L} \sum_i q_i^2 + \sum_{i < j} q_i q_j \left[\frac{1}{(r_{ij}^2 + z_{ij}^2)^{1/2}} + \sum_{k=0}^{\infty} \frac{(-1)^k r_{ij}^{2k}}{L^{2k+1} (2k!!)^2} \left\{ \Upsilon_{2k} \left(1 + \frac{z_{ij}}{L}\right) + \Upsilon_{2k} \left(1 - \frac{z_{ij}}{L}\right) \right\} \right]. \quad (3.13)$$

Now we can easily calculate the forces needed for our MD simulation by differentiating this potential as stated in Equ. (3.1).

3.2 Spectroscopy

Frequencies of intramolecular vibrations are influenced by the local solvent environment. Hence, studying absorption spectra which are determined by molecular vibrations, can yield information about the structure and dynamics of a system. Experimental physicists developed highly sophisticated methods to measure spectra, which give us the opportunity to verify the results obtained by simulations or check if the experimental system was prepared in the right way.

3.2.1 Infrared spectroscopy

Infrared spectroscopy concentrates on the infrared spectrum of a substance. The physics which influences this part of the spectrum are the vibrational and rotational movements of molecules. The intramolecular vibrations are influenced by surrounding molecules through an electric field. The charge distribution of neighbour molecules is not uniform and thus the electrostatic interaction between these charge distributions influences intramolecular bonds. These bonds are much stronger than for example intermolecular hydrogen bonds, but the influence of the hydrogen bond topology is sufficient to shift vibrational frequencies.

3.2.2 Raman spectroscopy

Another possibility to get information about the rotational and vibrational behaviour of a system is Raman spectroscopy. The Raman effect occurs when a photon excites a molecule to a higher energy state. Afterwards the

molecule emits a photon and relaxes into a different vibrational or rotational state as before. This results in an energy transfer between the excitation energy and the vibrational or rotational energy. This energy transfer changes the frequency of the emitted photon. With Raman spectroscopy one measures this shift of the photo frequency away from the usual non Raman influenced excitation frequency.

3.2.3 Optical absorption coefficient

The optical absorption coefficient $\alpha(\omega)$ describes how much Energy E is absorbed by a substance per time, if it is exposed to an energy flux S . This absorption coefficient is a function of the frequency ω of the incident light and the electric dipole-dipole time correlation function. Its definition is:

$$\alpha(\omega) = (dE/dt)_{abs}/S \quad (3.14)$$

Zwanzig derived a formula for the optical absorption coefficient [23].

Absorption involves an energy gain of the system. Therefore we calculate the energy change of the system to obtain $\alpha(\omega)$. The energy change is the difference in the energy times the transition rate between the energy levels of the molecule. We know that the transition rate is proportional to the frequency from Fermi's golden rule [21]. E_f are the energy levels of the system, ω_{fi} is the frequency of a photon emitted or absorbed as a cause of a transition from energy level f to energy level i . To take into account the probability of the different states we use the Boltzmann weight ρ_i and sum over all f and i .

$$\frac{dE}{dt} = \sum_{f,i} \rho_i (E_f - E_i) \omega_{fi} \quad (3.15)$$

We can write down the transition rate ω_{fi} by using the delta representation of Fermi's golden rule [21]:

$$\omega_{fi} = \frac{\pi}{2\hbar} |\langle f|V|i \rangle|^2 \{ \delta(E_f - E_i - \hbar\omega) - \delta(E_f - E_i + \hbar\omega) \} . \quad (3.16)$$

Here, V is the Hamiltonian which perturbs the system. Using this expression and writing $\hbar\omega$ instead of $(E_f - E_i)$ we obtain:

$$\frac{dE}{dt} = \frac{\pi}{2} \omega \sum_{f,i} \rho_i |\langle f|V|i \rangle|^2 \{ \delta(E_f - E_i - \hbar\omega) - \delta(E_f - E_i + \hbar\omega) \} . \quad (3.17)$$

By switching the indices in the second delta function, we can write $\frac{dE}{dt}$ as:

$$\frac{dE}{dt} = \frac{\pi}{2}\omega \sum_{f,i} (\rho_i - \rho_j) \langle f|V|i \rangle^2 \delta(E_f - E_i - \hbar\omega) . \quad (3.18)$$

Next, we want to eliminate ρ_j . To do this, we need the equation which relates the Boltzmann distributions ρ to each other:

$$\rho_f = \rho_i \exp(-\beta(E_f - E_i)) . \quad (3.19)$$

Inserting this expression into Equ. (3.18) leads to:

$$\frac{dE}{dt} = \frac{\pi}{2}\omega (1 - \exp(-\beta\hbar\omega)) \sum_{f,i} \rho_i \langle f|V|i \rangle^2 \delta(E_f - E_i - \hbar\omega) . \quad (3.20)$$

Instead of the Delta distribution we can use its integral representation defined as:

$$\delta(E - \hbar\omega) = \frac{1}{2\pi\hbar} \int_{-\infty}^{+\infty} dt \exp(-i\omega t) \exp(itE/\hbar) . \quad (3.21)$$

For the next step, we also need the Heisenberg representation for the time dependence of the perturbing Hamiltonian:

$$V(t) = \exp(itH/\hbar) V(0) \exp(-itH/\hbar) . \quad (3.22)$$

Using these two expressions, Equ. (3.20) becomes:

$$\frac{dE}{dt} = \frac{\omega}{4\hbar} \left(1 - \exp(-\beta\hbar\omega)\right) \int_{-\infty}^{+\infty} dt \sum_{f,i} \rho_i \langle i|V(0)|f \rangle \langle f|V(t)|i \rangle . \quad (3.23)$$

The $\langle f|$ are orthogonal to each other and thus cancel out. The sum over all i produces the expected equilibrium value which simplifies the expression to:

$$\frac{dE}{dt} = \frac{\omega}{4\hbar} (1 - \exp(-\beta\hbar\omega)) \int_{-\infty}^{+\infty} dt \exp(-i\omega t) \langle V(0)V(t) \rangle_{eq} . \quad (3.24)$$

To obtain the classical limit of the above equation we Taylor expand the exponential function to the first order in \hbar :

$$\exp(-\beta\hbar\omega) \approx 1 - \beta\hbar\omega . \quad (3.25)$$

We insert this expression in Equ. (3.24), and carry out the limit $\hbar \rightarrow 0$, which results in:

$$\frac{dE}{dt} = \frac{\omega^2 \beta}{4} \int_{-\infty}^{+\infty} \exp(-i\omega t) \langle V(0)V(t) \rangle_{eq} . \quad (3.26)$$

The perturbation $V(t)$ equals the dot product of the incident light wave $\vec{E}_0 \cos(\omega t)$ times the electric dipole moment of the system $\vec{M}(t)$ which interacts with the light wave:

$$V(t) = \vec{E}_0 \cos(\omega t) \cdot \vec{M}(t) . \quad (3.27)$$

We insert this expression in Equ. (3.24). The cosine vanishes because of the time averaging and we obtain:

$$\alpha(\omega) \propto \frac{dE}{dt} \propto \omega^2 \beta \int_{-\infty}^{+\infty} dt \exp(-i\omega t) \langle M(0)M(t) \rangle_{eq} . \quad (3.28)$$

For simplicity we dropped the dependence on E_0 and other constant factors in the last equation, since we are only interested in the shape of the spectrum and not in its absolute magnitude.

3.2.4 Calculating IR absorption spectra

In each time step of our simulation we get a different force on every hydrogen and so a different F . The Schrödinger equation then gives us a different energy eigenvalue every timestep which influences our electric dipole moment $M(t)$.

$$M(t) = r_{oh}(t) \exp\left\{-\frac{i}{\hbar} \int_0^t dt' E_1(t') - E_0(t')\right\} \quad (3.29)$$

By inserting this in Equation (3.28) and taking into account the vibrational lifetime T_1 of an OH excitation we obtain the following expression for the infrared line shape:

$$I(\omega) \propto \omega \int_{-\infty}^{\infty} dt e^{i\omega t} \left\langle \exp\left[-\frac{i}{\hbar} \int_0^t dt' E_1(r(t')) - E_0(r(t'))\right] \right\rangle \langle r_{OH}(t) * r_{OH}(0) \rangle e^{-|t|/2T_1} \quad (3.30)$$

3.3 Time correlation functions

Time correlation functions are important to analyze the dynamics of a system. The time average of a quantity A during a period τ is defined by:

$$\langle A \rangle = \frac{1}{\tau} \int_0^\tau dt A(t) . \quad (3.31)$$

We subtract this time average $\langle A \rangle$ from the quantity $A(t)$ and obtain:

$$\Delta A(t) = A(t) - \langle A \rangle . \quad (3.32)$$

We can define a correlation function for every time dependend quantity, which gives us information about how fast this quantity changes in time.

We define this correlation function as follows:

$$C(t) = \frac{1}{\tau} \int_0^\tau dq \Delta A(q) \Delta A(t + q) . \quad (3.33)$$

This time correlation function is called the autocorrelation function of A , because it correlates the quantity A with the same quantity after a time t .

Chapter 4

Numerical results

4.1 Simulation details

We performed molecular dynamics simulations by integrating Newton's equations of motion using the Verlet algorithm [24]. The SHAKE algorithm kept the molecules rigid [25]. The details of these methods are described in Chapter 3. We chose a time step of 1.4 fs to keep the energy fluctuations sufficiently small at a temperature of 298 K. The water model we used was SPC/E [16]. The system consisted of one HOD and 30 D₂O. All these molecules were confined inside a (6,6) carbon nanotube with a diameter of 8.1 Å C-C distance. The nanotube was modelled by applying an external polynomial potential to the water molecules. Details about the carbon nanotube model can be found in Chapter 2.4. We applied periodic boundary conditions in the direction of the cylinder axis. To simulate an infinitely long tube we calculated a 1D lattice sum, which we previously derived in

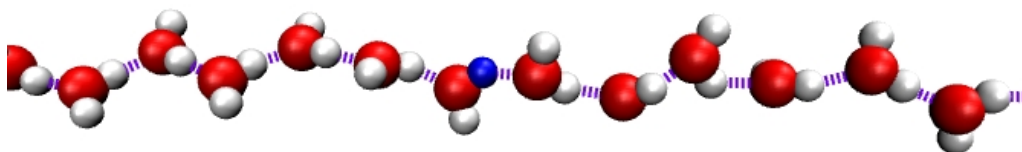


Figure 4.1: A part of the system. Blue atom: hydrogen, white atoms: deuterium, red atoms: oxygen, purple lines: hydrogen bonds.

Chapter 3.1.3 [26]. As 1D density (particle number/length of the box) we used 0.385 \AA^{-1} , as calculated by Striolo, Chialvo, Gubbins for the (6,6) carbon nanotube at ambient conditions [27]. A snapshot of a part of the system is shown in Fig. 4.1. The water molecules align in a chain, and are linked through hydrogen bonds.

4.2 Dipole-dipole time correlation function

Time correlation functions play an important role in nonequilibrium statistical mechanics and linear response theory. Since optical absorption is a nonequilibrium process, where the system is driven out of equilibrium by the electromagnetic wave, it is essential to calculate the dipole-dipole time correlation function of the system [23].

In Chapter 3.2.3 we derived that we need this correlation function to calculate the infrared spectrum, furthermore it serves as a measure of the timescale associated with the dynamics of the system.

We insert the dipole moment vector $\vec{D}(t)$ of the HOD molecule in Equ. (3.33) to obtain the dipole-dipole time correlation function $C_D(t)$:

$$C_D(t) = \frac{1}{\tau} \int_0^\tau dq \Delta \vec{D}(q) \cdot \Delta \vec{D}(t+q) . \quad (4.1)$$

Köfinger, Hummer and Dellago showed that the water molecules form an ordered chain [1]. We used this result for the starting configuration of our system and we expect that the average dipole moment $\langle \vec{D} \rangle$ is non-zero for our simulation trajectories, which are on the nanosecond scale. However, for long times the average dipole moment $\langle \vec{D} \rangle$ tends to zero, because of the non-vanishing chance of a global flipping event, during which the dipole moment of the major part of the molecules flips in the opposite direction.

To calculate C_D we used this property of the system and set $\langle \vec{D} \rangle$ to zero, although we do not observe it in our molecular dynamics simulations. Our trajectories usually were on the nanosecond scale and are much too short to see such a global flipping event.

In Fig. 4.2 you see the resulting dipole-dipole time correlation function. This correlation function is expected to show an exponential decay to zero with a characteristic time equal to the flipping time. This decay is not

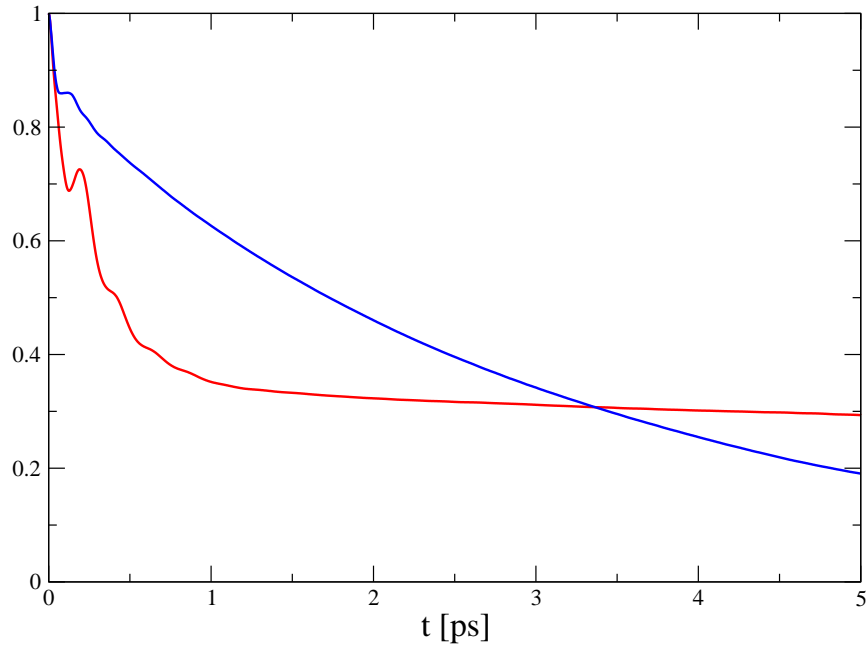


Figure 4.2: Dipole-dipole time correlation function (red) and Frequency autocorrelation function (blue)

visible in Fig. 4.2, because on the time scale of our simulation flipping events are very rare.

4.3 Oxygen-oxygen and hydrogen-hydrogen radial distribution functions

The radial distribution function $g(r)$ is the expectation value of the particle number divided by the particle number for a homogeneous medium with a density ρ within a thin spherical shell of radius r ,

$$g(r) := \frac{\langle \sum_{j \neq i} \delta(r - r_{ij}) \rangle}{4\pi r^2 \rho N}. \quad (4.2)$$

Here N is the number of particles in the system and r_{ij} is the distance between particle i and particle j .

In our system we have three types of particles: oxygen atoms, deuterium atoms and hydrogen atoms. Since we are calculating the spectrum of the single HOD molecule in our system, we are interested in the distances of the D_2O molecules to the single HOD. A useful function to quantify the structure of the system is the oxygen-oxygen radial distribution function.

As one can see in Fig. 4.3, there is a very sharp peak, centered at 2.45 \AA in the O-O radial distribution function, which means that the first neighbour molecules are located in a small region. At larger distances we see further peaks, which correspond with the next neighbour molecules. With larger distances the peaks widen, because the particles become uncorrelated.

To analyze the structure of the system in more detail we calculate the hydrogen-hydrogen radial distribution function. For the bonded hydrogens we expect pretty much the same picture as for the oxygens, because the bonded hydrogens are directly linked to the oxygens through the hydrogen bonds. Therefore, we concentrate on the free hydrogens. We expect that

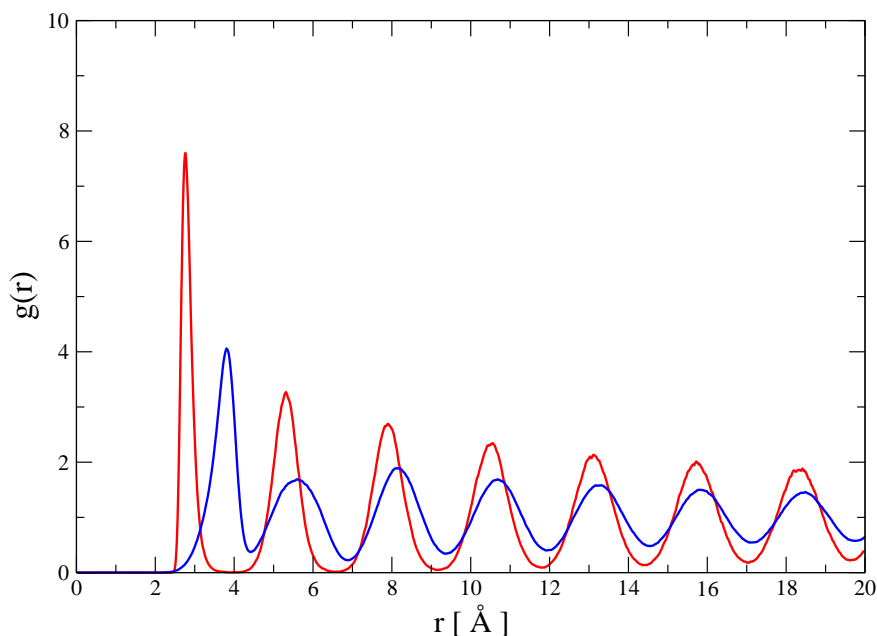


Figure 4.3: red: $O - O$ radial distribution function, blue free H-H radial distribution function

they are more mobile and show a different behavior than the oxygens.

The first neighbour shell of the free hydrogens is farther away than that of the oxygens, see Fig. 4.3. This can be explained by the fact that the hydrogens carry positive charges and are influenced by their repulsive forces. Thus the free hydrogens rotate in the chain, trying to maximize the distance from each other.

4.4 OH angle pair distribution functions

To get more detailed information about how the free hydrogen and deuterium atoms arrange, we calculated OH angle distribution functions. To do this, we first define φ_n as the azimuthal angle of the n^{th} neighbour molecule's OH vector. Then we calculate distributions of the angles $|\varphi_0 - \varphi_n|$.

The red and orange curves for high temperatures and low densities in

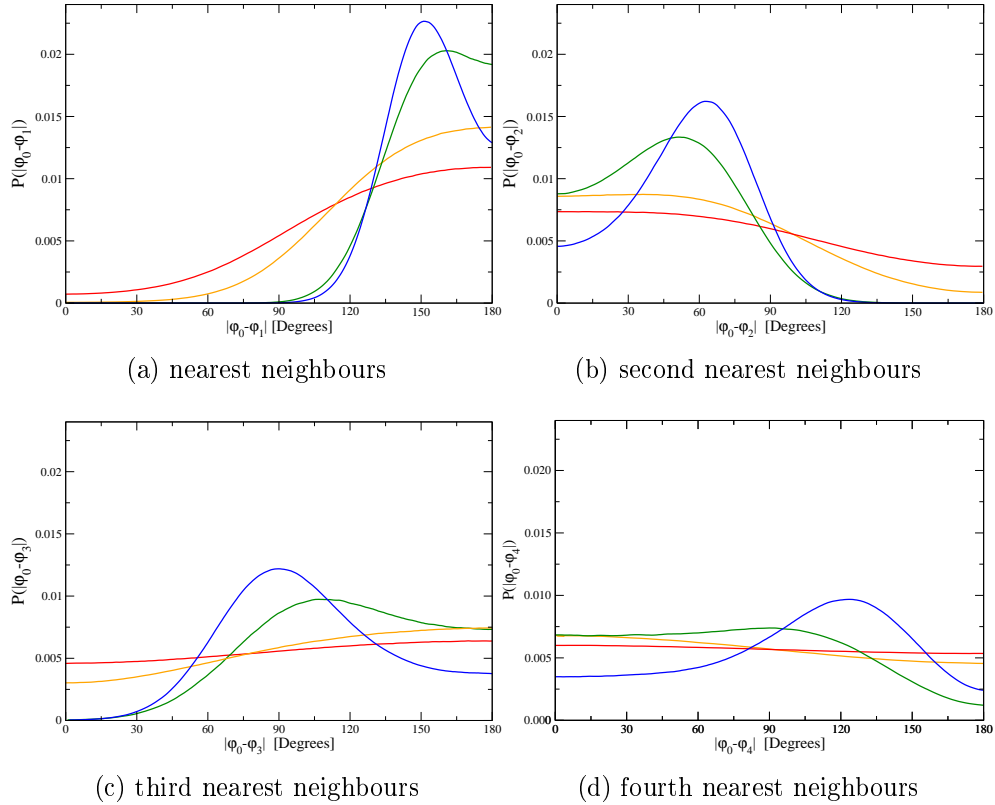


Figure 4.4: OH angle distribution functions between different neighbour molecules, blue: 50 K, green: 110 K, orange 200 K, red 298 K

Fig. 4.4 show the expected results. The free atoms try to maximize the distances from each other, aligning in 180° angles.

The blue and green curves for low temperatures and higher densities show a different behavior. At these conditions the influence of the second nearest neighbours becomes important, and the OH angles of the nearest neighbours decreases significantly.

At lower temperatures the most probable OH angle between the nearest neighbours is around 150° , between the second nearest neighbours 60° , between the third nearest neighbours 90° and the fourth nearest neighbours 120° . We calculated only angles between 0 and 180° and therefore lost information about the actual orientation. If we assume for angles with an even n : $|\varphi_0 - \varphi_n| = 360 - |\varphi_0 - \varphi_n|$. We get the angles: $0^\circ, 150^\circ, 300^\circ, 90^\circ, 240^\circ$. We notice that they are equidistant on a circle, which suggests a helical structure of the system with an angle change per molecule of 150° . We illustrate such a configuration in Fig. 4.5.

For high temperatures the angle correlation nearly vanishes at the fourth nearest neighbour, whereas at low temperatures we still notice a significant maximum for the most probable angle.

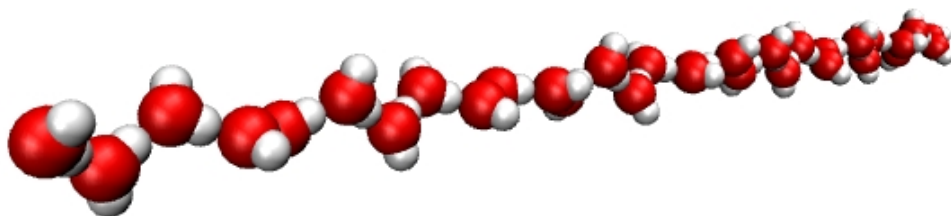


Figure 4.5: Helical structure of a single-file water chain, with an azimuthal angle change of about 150° per molecule

4.5 E-field distributions

As derived in Chapter 2.5, the OH vibrational frequency is to first order determined by the distributions of E_H , the electrostatic field at the hydrogen in direction of the oxygen, and to E_O , the electrostatic field at the oxygen in direction of the hydrogen. These fields divided by the masses of the hydrogen and the oxygen and multiplied by a constant, result in the first order term F , see Equ. (2.21). Thus, E_H is the dominating quantity, because the oxygen is 16 times heavier than the hydrogen.

The E_H distribution in Fig. 4.6 shows two peaks, one centered at -0.1 V\AA^{-1} and the other at -2.1 V\AA^{-1} .

These two peaks can be explained by looking at the setting of one single HOD (see Fig. 4.7). The molecule is neighboured by two D_2O 's. The hydrogen of the HOD molecule donates a hydrogen bond to one D_2O and the oxygen accepts one of the other D_2O molecule. The D atom is free, without any hydrogen bonding.

Every several picoseconds a flipping event occurs where the hydrogen and the deuterium atoms switch their positions. The hydrogen breaks up the hydrogen bond with the neighbouring D_2O and the deuterium of the HOD donates the hydrogen bond to the D_2O . Now the hydrogen is free.

The peak centered at -0.1 V\AA^{-1} is associated with the time when the hydrogen is free, see Fig. 4.7a and the other peak is associated with the time when the hydrogen is bonded, see Fig. 4.7b. We have also tested this by collecting statistics separately. One distribution is for the hydrogen, when it is nearer to the neighbouring oxygen of the D_2O than the deuterium and another one is for the other way around. With this method we obtained two distribution functions, one with a single peak centered at -0.1 V\AA^{-1} and one with a single peak centered at -2.1 V\AA^{-1} . The integral over each of the functions must be the same, because the probability for the deuterium being nearer to the neighbouring oxygen than the hydrogen is the same as vice versa. This is because these expectation values are independent of the masses of the atoms, which is the only quantity that distinguishes them.

The E_O distribution shows similar peaks as the E_H distribution. The oxygen does not flip between different hydrogen bond configurations and therefore should not show two well separated peaks. However, since we are

measuring the electrostatic field always in direction of the OH vector we get a peak centered at $-1.1 \text{ V}\text{\AA}^{-1}$ associated with a bonded hydrogen and a peak centered at $-0.05 \text{ V}\text{\AA}^{-1}$ associated with a free hydrogen, in analogy to the distribution of E_H .

The E_H bond peak is located at negative field strength, because the force on the hydrogen has its origin mainly in the oxygen of the neighbouring

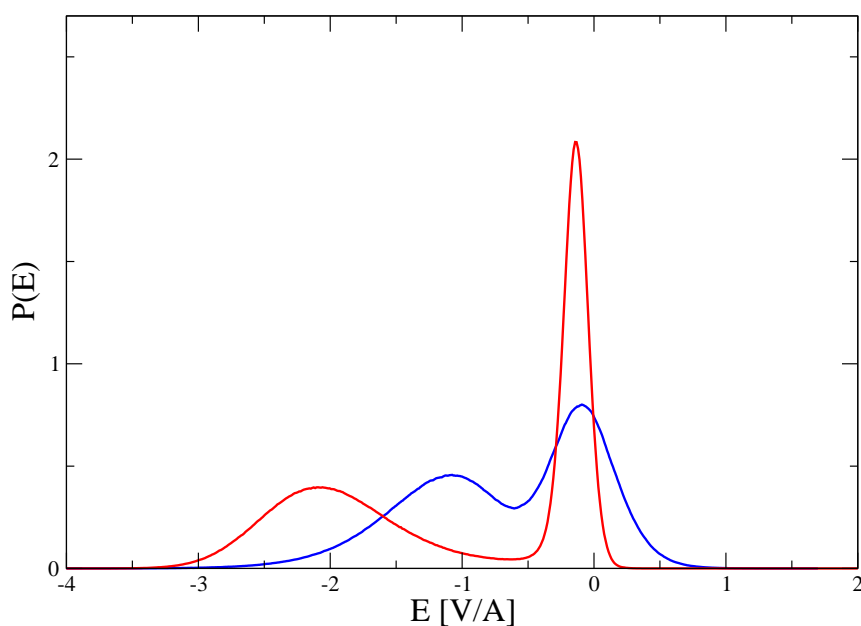
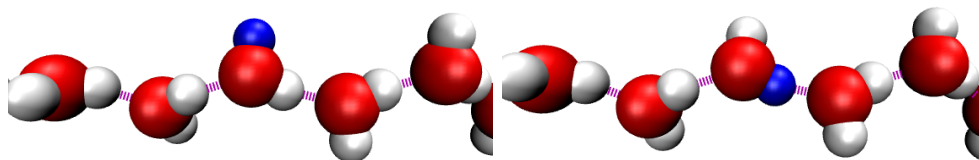


Figure 4.6: Red: E_H distribution, blue: E_O distribution



(a) blue atom: free hydrogen

(b) blue atom: bonded hydrogen

Figure 4.7: The two different hydrogen bond configurations for the HOD molecule in nanopore water

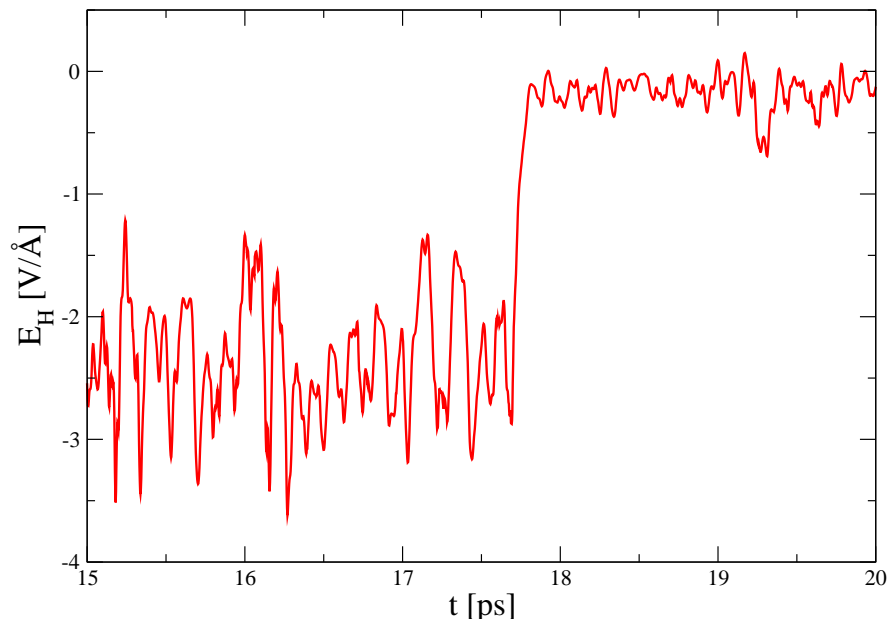


Figure 4.8: Time evolution of E_H at an arbitrary hydrogen during a switch from a bonded to a free state

molecule, which is attracting the hydrogen. We also notice that the free peak is much sharper than the bond peak. The fluctuations of the forces and also the magnitudes of the forces at the bonded hydrogen are much stronger than in the free hydrogen. We can see this in Fig. 4.8, which is an arbitrary example of $E_H(t)$ during a transition from a bonded to a free state. We also notice that the transition between the bonded and free state is very fast.

4.6 Frequency distribution

Since the OH vibrational frequency ω_{OH} is, to first order, mainly dependent on E_H , as we have seen in Chapter 2.5, we expect for the frequency distribution nearly the same shape as for the E_H distribution. The second order term G should not influence the shape of the spectra significantly. Eaves, Tokmakoff and Geissler obtained this result for bulk HOD in liquid D₂O

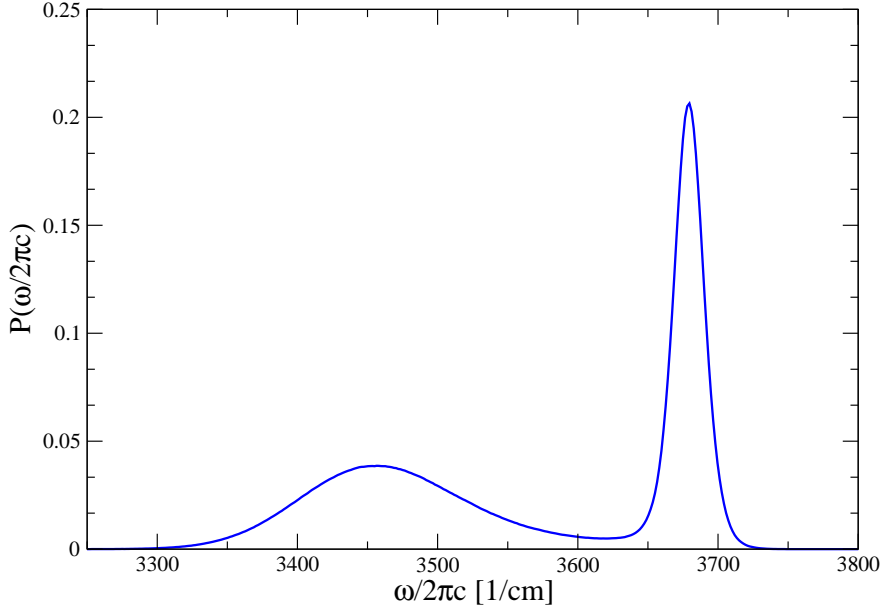


Figure 4.9: HOD stretch frequency distribution of nanopore water

[12]. They calculated a strong linear correlation between the OH frequency ω_{OH} and E_H .

Furthermore, first order perturbation theory has to be sufficient for the calculation of $\langle H_{sb} \rangle$ in Equ. (2.25) to get a linear dependence. If that is the case, the calculation of ω_{OH} results in a simple expression, see Equ. (2.26).

For the frequency distribution of the nanopore water system, see Fig. 4.9, we took account for the second order term G and also used second order perturbation theory. Despite this more accurate calculation, the frequency distribution has a very similar shape to the E_H distribution in Fig. 4.6, which confirms the minor importance of G and second order perturbation.

4.7 E_H - ω_{OH} correlation

Next we will quantify how strongly E_H is correlated to the OH vibrational frequency ω . For this purpose, we calculate the correlation between E_H and ω_{OH} in the nanopore water system. We count how often a certain

E-field leads to a certain vibrational frequency, draw this statistics in a two-dimensional plain and colour it according to the probability.

As shown in Fig. 4.10, the joint distribution of E_H and ω_{OH} has a nearly straight and very narrow form. Therefore it is possible to determine an approximate relation between the E-field and ω_{OH} , by fitting a linear curve to this data. Smith, Saykally and Geissler calculated the coefficients for this transformation for bulk water [28]. The coefficients for the single file water differ from them for bulk, because the influence of the second order term G is different. We are going to explain in Chapter 4.8 why this does not disrupt the linear behavior.

The relation for the nanopore water system is:

$$\omega = 155 \text{ cm}^{-1} \text{V}^{-1} \text{\AA} \times E_H + 3705 \text{ cm}^{-1} . \quad (4.3)$$

In comparison, the relation for bulk HOD in liquid D₂O determined by Smith, Saykally and Geissler is:

$$\omega = 160.514 \text{ cm}^{-1} \text{V}^{-1} \text{\AA} \times E_H + 3745 \text{ cm}^{-1} . \quad (4.4)$$

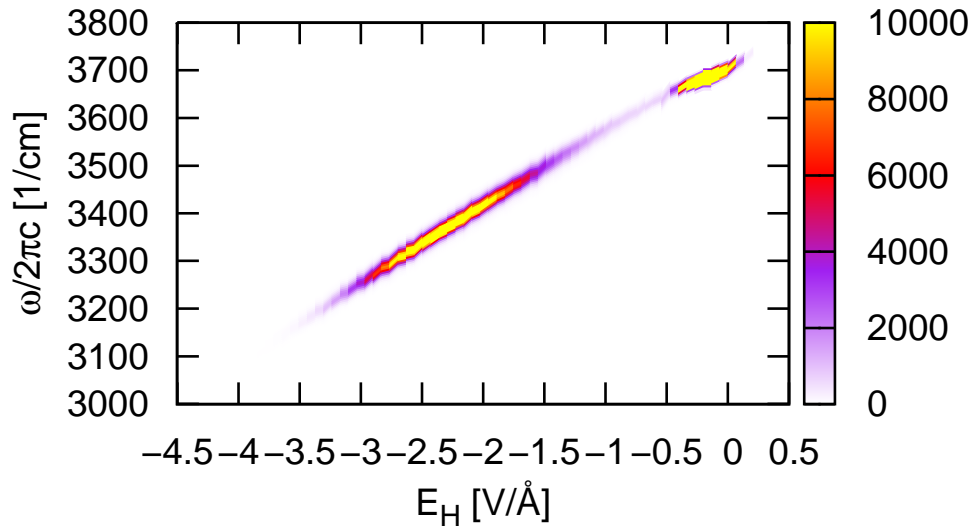


Figure 4.10: Color coded joint probability distribution of E_H and ω

Paesani, Xantheas and Voth recently also confirmed this linear dependency for bulk HOD in D₂O and HOD in H₂O by use of Centroid Molecular Dynamics with an Ab Initio-Based Force Field[29].

4.8 E_H - G correlation

To explain why the non-vanishing second order term G does not destroy the linear dependence between E_H and ω , we calculate the correlation between E_H and G . For these two quantities we also get a quite linear relation, see Fig. 4.11.

The vibrational frequency ω is a function of E_H and G :

$$E_{sbm} = F\langle n|Q|n\rangle + G\langle n|Q^2|n\rangle \approx \mu \hat{r}_{OH} \cdot \vec{E}_H \langle n|Q|n\rangle + G\langle n|Q^2|n\rangle. \quad (4.5)$$

For $G = 0$ we expect a linear correlation between ω and E_H . For $G \neq 0$ this linear dependence should break down. However, since the correlation between E_H and G is also linear, the transformation in Equ. (4.3) holds.

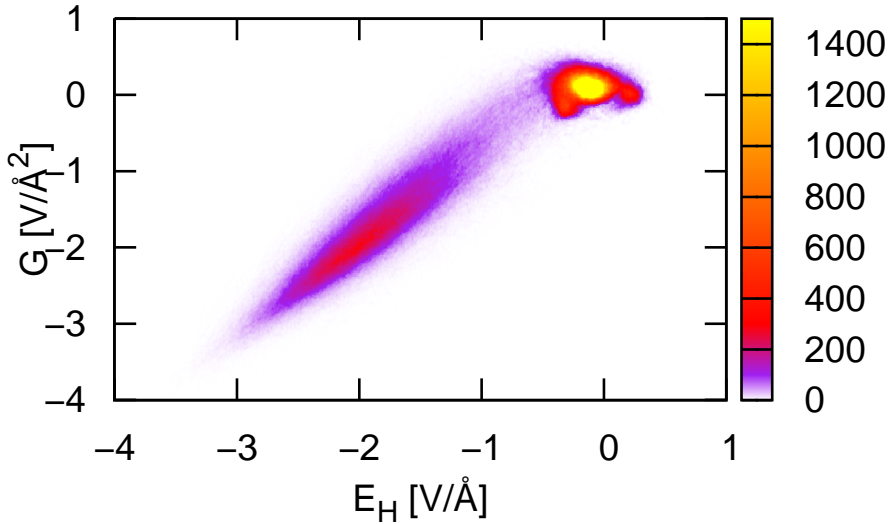


Figure 4.11: Color coded joint probability distribution for E_H and G

4.9 Temperature dependence

We also studied the temperature dependence of single-file water frequency distributions. We performed simulations at temperatures 450 K, 600 K, 900 K and 1500 K. The corresponding frequency distributions are shown in Fig. 4.12. Up to a temperature of 600 K one can distinguish between the free peak and the bond peak, which indicates stable hydrogen bonds and the single-file order. At higher temperatures the peaks merge into one single peak. Since thermal fluctuations become stronger, the water molecules become more mobile and the probability for stronger E-fields in the free peak increases. More and more defects occur in the chain and the bond peak disappears.

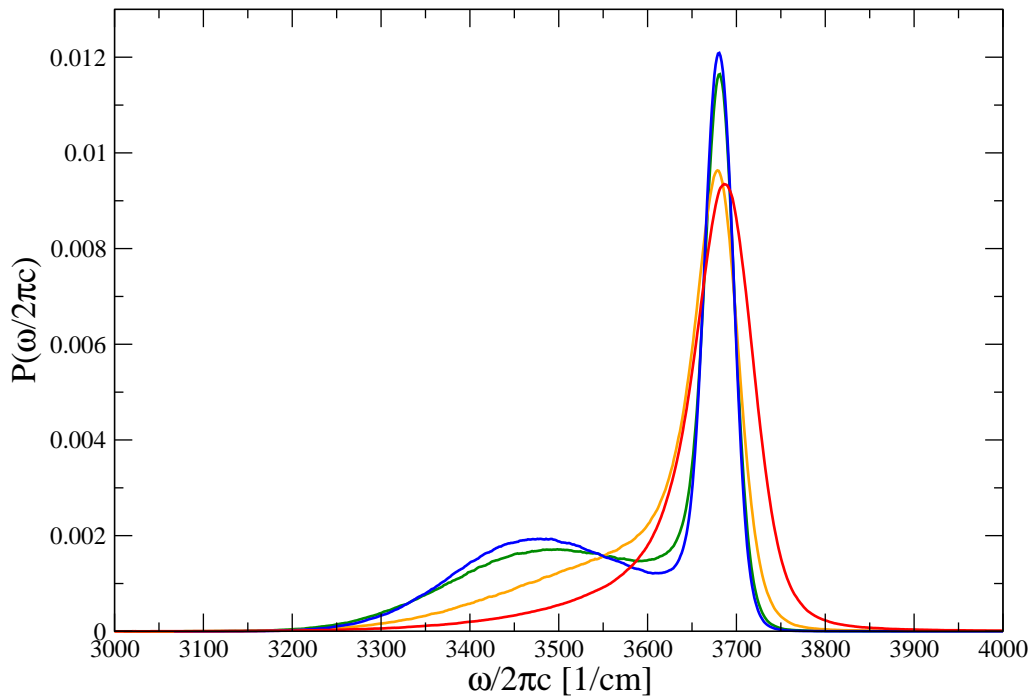


Figure 4.12: Frequency distributions for single-file nanopore water at different temperatures. Blue: 450 K, green: 600 K, orange: 900 K, red: 1500 K.

4.10 Infrared spectrum

The states of a molecule are perturbed while it is moving through a bath, due to the fluctuations in the force which act on its intramolecular bonds. Since the lifetime of the excitations is non-zero, the frequency of the emitted or absorbed photons is a time average. Furthermore, the mean values of a sample have always smaller variance than the individual variables. Therefore, infrared spectra are usually narrower than the corresponding frequency distributions. This effect is known as motional narrowing.

The vibrational lifetime T_1 of the OH bond in D_2O is on the same timescale as the decay of the frequency autocorrelation function, see Fig. 4.2. Therefore, motional narrowing cannot be neglected for the calculation of the nanopore water system's infrared line shape. As numerical value for T_1 we used an experimental result of pump-probe experiments by Loparo, Fecko, Roberts and Tokmakoff [30, 31].

The decay of the dipole-dipole time correlation function limits the narrowing effect. The interaction between the incident electromagnetic wave

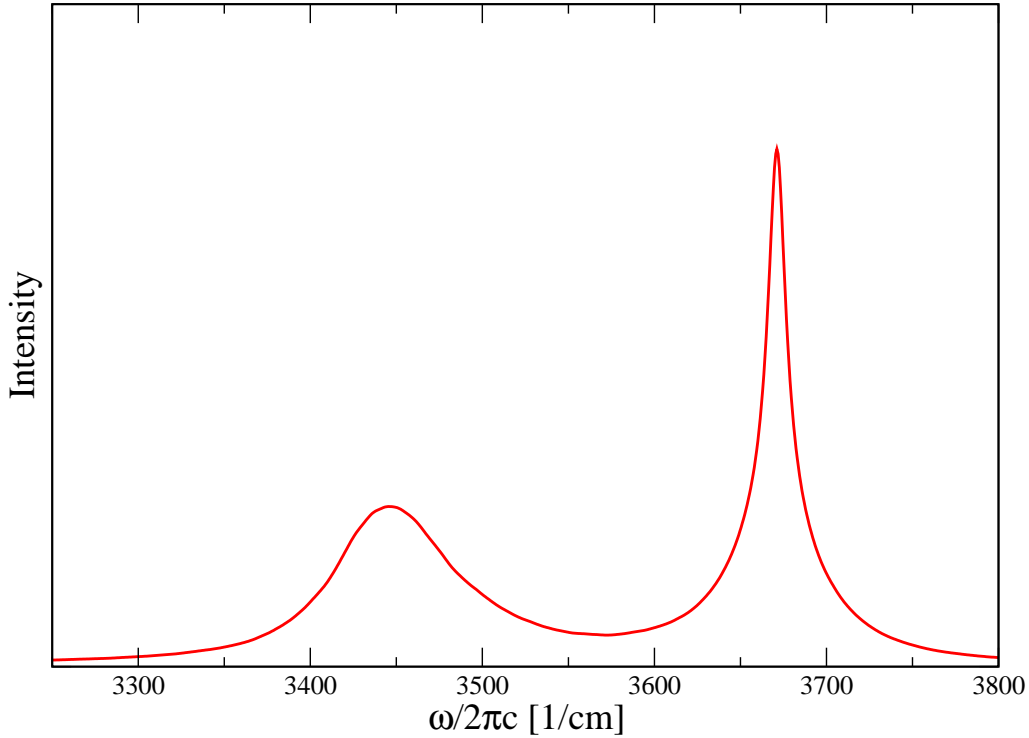


Figure 4.13: Infrared spectrum of the single-file nanopore water system

and the OH bond is described by the dot product between the wave's E-field vector and the OH bond's dipole vector. If these vectors are perpendicular, no energy is transferred and excitation is inhibited. Since the dipole-dipole time correlation function decays significantly on the femtosecond scale, we have to consider it in our calculations, see Fig. 4.2. A quantum mechanical description of the dipole moment is not necessary. Especially for the OH stretching, the classical representation of the dipole moment operator leads to even better results than the quantum mechanical approach [29, 32].

For very short excitation lifetimes the variation in the energies increases because of the uncertainty relation between energy and time. This leads to line broadening. We neglect this effect in our calculations, since the vibrational lifetime T_1 of the OH bond is about 750 fs, which is much too long to have a considerable effect on the energies [30, 31].

To calculate the infrared line shape, we used an expression by Zwanzig, derived in Chapter 3.2.3, and Eaves, Tokmakoff and Geissler adapted by use of a quantum mechanical time evolution operator, see Equ. (3.30), [23, 12]. This expression takes into account the effects described above, except for the line broadening.

The shape of the IR-spectrum in Fig. 4.13 differs from the frequency distribution shown in Fig. 4.9 but is qualitatively the same. The bond peak has a line width of 85 cm^{-1} and the free peak has 15 cm^{-1} . The motional line narrowing compared to the frequency distribution is about 38 % for the bond peak and about 33 % for the free peak. Compared to the motional narrowing of 30 % in bulk water, this effect is more pronounced in the single-file nanopore water system [28].

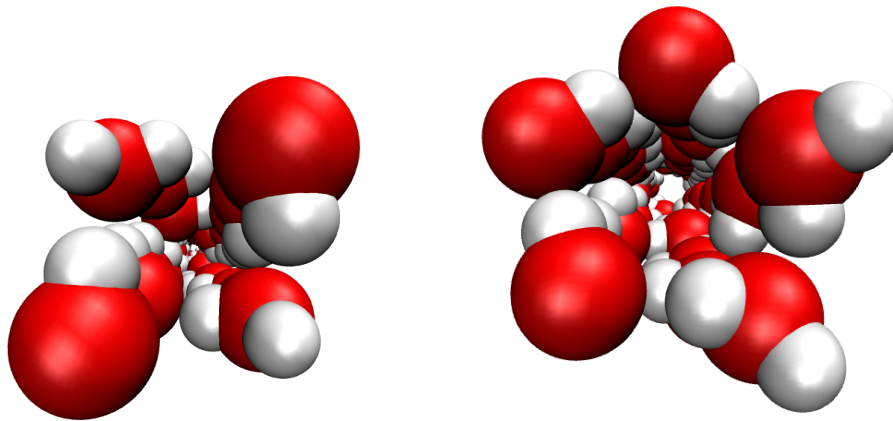
4.11 Wide carbon nanotubes

To date no method is available to produce carbon nanotubes of one single kind. Experimentators have to deal with an ensemble of carbon nanotubes with different diameters. Therefore, we simulated water in several wider carbon nanotubes with diameters ranging from 10.9 \AA to 13.6 \AA . By calculating the infrared spectra of the OH stretch we want to check whether it is possible to distinguish between the single file order in the (6,6) tube and the water configurations in wider tubes through spectroscopy. To model these

tubes we adapted the tube potential as described in Chapter 2.4.

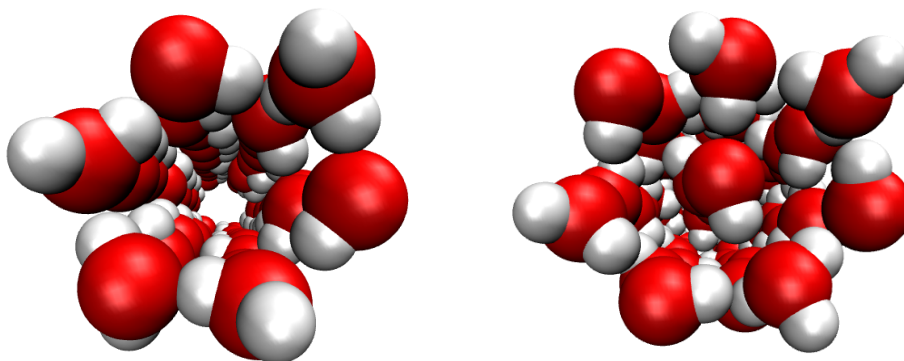
4.11.1 Structure

Water in tubes with diameters larger than 10.9 \AA shows a great variety of different structures. N -gonal ring tubes and also multilayer tubes of water are common configurations. Koga, Gao, Tanaka, and Zeng even found indications for a first order phase transition between liquid and these ice-like structures [8].



(a) (8,8) CNT, tetragonal

(b) (9,8) CNT, pentagonal



(c) (9,9) CNT, hexagonal

(d) (10,10) CNT, DL heptagonal/single

Figure 4.14: Ice-like structures in CNT's, view along the tube axis

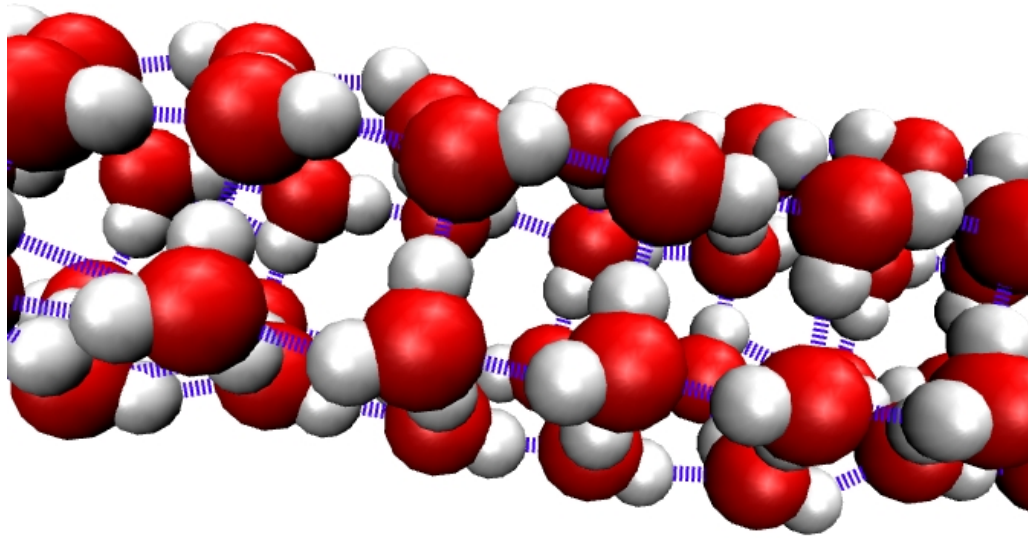


Figure 4.15: Hydrogen bond network in a hexagonal water tube

Under these carbon nanotube confinements water tries to maximize the number of hydrogen bonds in the following way: The water molecules form a tube, where each of them receives two hydrogen bonds, one by a neighbouring molecule in the same ring, one by a molecule of a neighbouring ring. Consequently it also donates two hydrogen bonds (again, one to a water molecule member of the same ring one to a molecule of a neighbouring ring), see Fig. 4.15. From now on we call hydrogens, that donate bonds in their own ring, intra-ring hydrogens, and hydrogens, that donate bonds to a neighbouring ring, inter-ring hydrogens.

At higher densities or larger tube diameters double layer (DL) water tubes form. In this case, a tube with a smaller diameter is located inside a larger one, see Fig. 4.14d. Also triple layer tubes were observed in simulations [9].

Pair correlation functions

To quantify the structure of such water configurations we chose the tetragonal water tube in a (8,8) CNT as an example. We calculated the oxygen-oxygen pair correlation function.

For distances larger than 7.5 Å we see single peaks, each peak representing one tetragonal neighbour ring. For smaller distances the O-O pair

CNT	Diameter Å	Density Å ⁻³	Structure	Temp K
(8,8)	10.9	1.41	tetragonal	295
(9,8)	11.5	1.68	pentagonal	295
(9,9)	12.2	1.93	hexagonal	295
(10,10)	13.6	2.28	disordered	295
(10,10)	13.6	3.27	DL heptagonal/single	220

Table 4.1: Simulated nanopore water systems

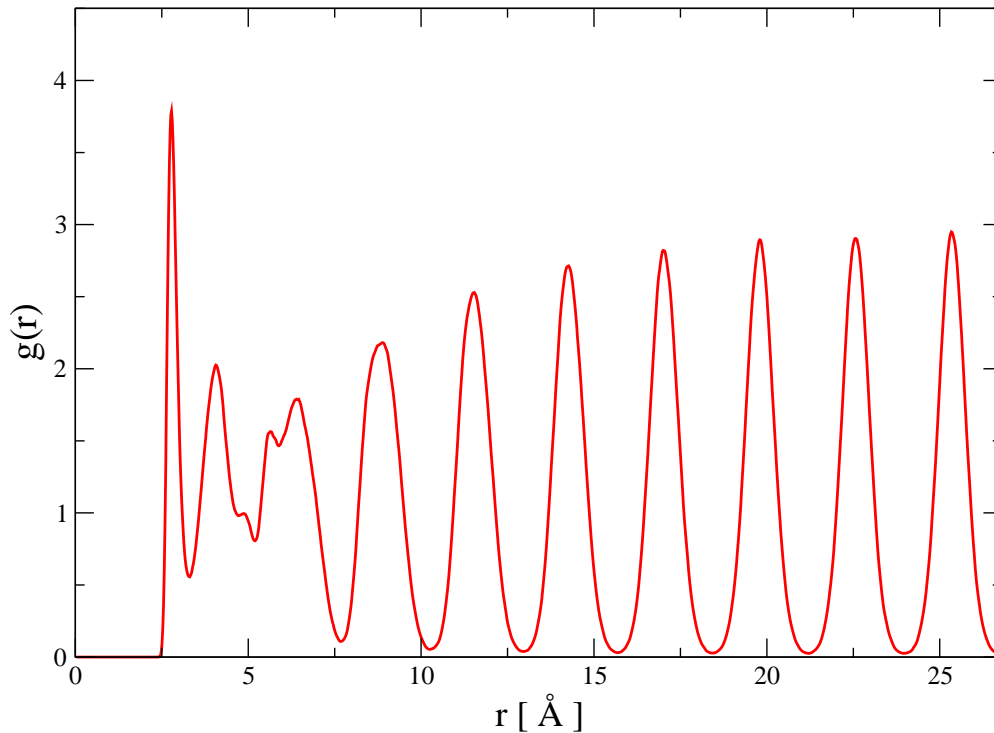


Figure 4.16: O-O pair correlation function of a tetragonal water file

correlation function resolves the intra-ring structure and we observe multiple peaks within the range of the first and second neighbour ring.

4.11.2 Frequency distributions and spectra

Water in wider carbon nanotubes forms a cylindracal structure with a hydrogen bonding network as described in the above paragraph. Each hydrogen has a quite similar environment. Nevertheless there is a slight difference between a inter-ring hydrogen and a intra-ring hydrogen. This is an effect

due to the curvature of the cylindrical water configuration and the HOH angle differing from 90° .

We calculated frequency distributions and infrared spectra of water under different tube confinements and temperatures, see Fig. 4.17.

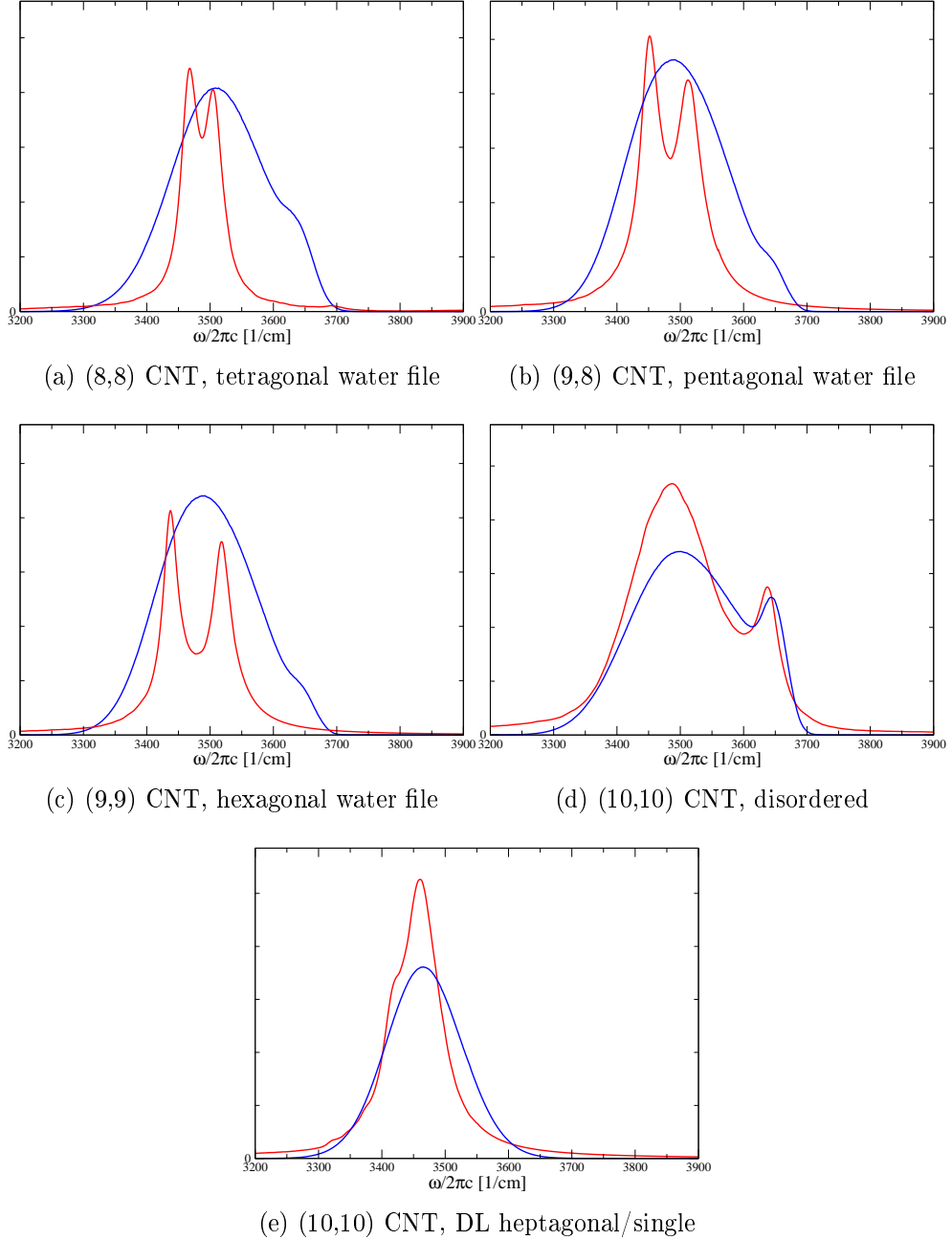


Figure 4.17: Frequency distributions(blue) and infrared spectra(red) of water under different (n,n) carbon nanotube confinements

Tetragonal, pentagonal and hexagonal structure

The frequency distributions for the tetragonal, pentagonal and hexagonal structure are single peaks with a slight shoulder on the blue side of the peak. They do not show a clear indication for a separation into two types of hydrogens, see Fig. 4.17a-4.17c.

However, the infrared spectra show two peaks close to each other. We identified the low(high) frequency peak as intra-ring (inter-ring) hydrogens by collecting separated statistics. This obviously means, that the motional narrowing effect revealed the presence of two types of hydrogens. For these ice-like water structures the narrowing effect is slightly stronger compared to single-file water, because of a slower decay of the dipole-dipole time correlation function. We conclude, that the frequency distributions are a sum of two peaks, which are too wide to be distinguished in the overall distribution. This further explains the slight shoulder in the frequency distributions, which is a result of slight asymmetries between the inter-ring and intra-ring peaks.

Compared to the results of Byl et al. [33] our intra-ring peaks are blue shifted by about 60 cm^{-1} . Byl et al. calculated their spectra at 123 K and used a flexible water model. At these temperatures it is very likely that the SPC/E model becomes inaccurate, but we expect it to be adequate in our temperature range, see Table 4.1.

Disordered Water

We found SPC/E water to be disordered in a (10,10) CNT at 295 K. In the frequency distribution and in the infrared spectrum we observe a broad peak with a small peak attached at the blue side, see Fig. 4.17d. Motional narrowing is inhibited due to the fast decay of dipole-dipole correlations. The broad peak is associated with bonded hydrogens. Due to strong fluctuations in this liquid-like state, hydrogens break their bonds and rotate towards the edge of the tube. This explains the smaller high-frequency peak.

Double Layer heptagonal/single structure

As an example for a double layer structure we calculated the spectrum of water inside a (10,10) CNT at 220 K. In this case, a single file water chain forms at the center of the tube. It is encircled by a heptagonal water tube. Note that the properties of the single file chain are very different from the single-file chains in (6,6) CNTs described above.

Neither the frequency distribution nor the infrared spectrum show a clear indication of different hydrogen types for this double layer configuration, see Fig. 4.17e. Nevertheless the infrared spectrum has a small shoulder on the red side, which suggests that the spectrum is a sum of multiple contributions.

4.12 Water dimer

We also studied the water dimer, a system consisting of two water molecules. In the lowest energy configuration, one molecule donates a hydrogen bond to the other. The former we call the donating molecule, and the latter we call the accepting molecule. By looking at a typical configuration, see

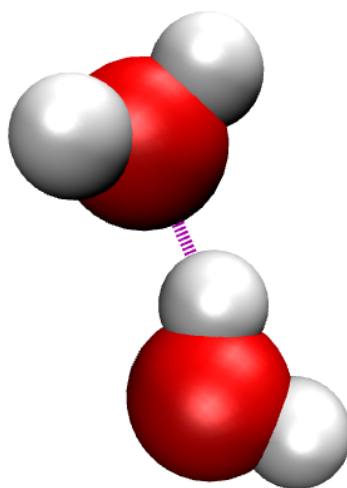


Figure 4.18: A snapshot of a water dimer

Fig. 4.18, one expects a similar OH vibrational spectrum as for the single-file water system, see Fig 4.9. The forces acting on the hydrogens of the donating molecule are alike the forces acting on a molecule within a single-file water chain. One hydrogen is bonded and one hydrogen is mobile with only a weak force acting on it. The forces on the hydrogens of the accepting molecule are qualitatively different. This molecule accepts a hydrogen bond and both of its hydrogens are not bonded.

The frequency distribution we determined shows three peaks, see Fig. 4.19a. The broad low frequency peak at 3567 cm^{-1} has a similar shape as the bond peak in the frequency distribution of single-file water in Fig. 4.9. We expect it to be associated with the bonded hydrogen of the donating molecule. Therefore, the high frequency peak at 3712 cm^{-1} has to be related to the free hydrogen of the donating molecule, because the integrals over the

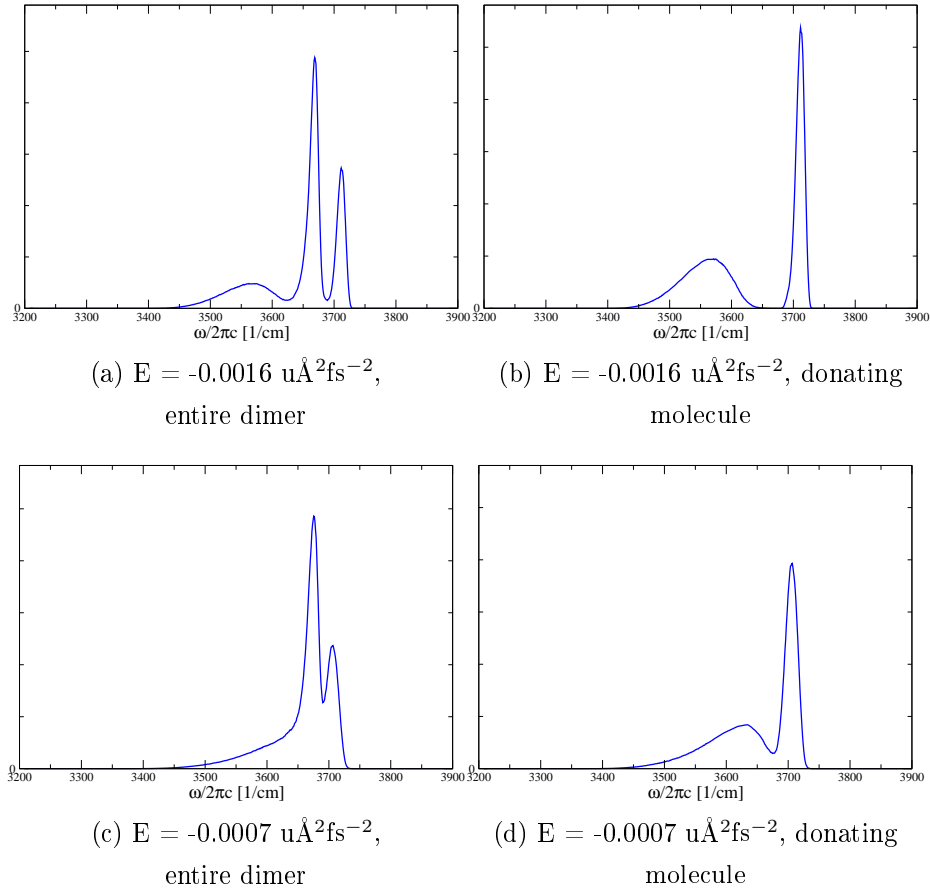


Figure 4.19: Frequency distributions of the water dimer at different energies

contributions of the donating molecule and the accepting molecule must be equal. This leaves only the possibility for the mid frequency peak at 3670 cm^{-1} to be associated with the free hydrogens of the accepting molecule. We also tested this interpretation by collecting separated statistics for the donating and the accepting molecule. We plotted the contribution to the frequency distribution of the donating molecule in Fig. 4.19b, which confirms our conclusions.

We also simulated the water dimer at a higher energy, see Fig. 4.19c. In this case the peaks broaden and the low frequency peak merges with the mid frequency peak. Again, by collecting separated statistics we excluded the spectrum of the donating molecule. Despite the stronger fluctuations, one can still identify the peaks for the bonded and the free hydrogen, see Fig. 4.19d.

Chapter 5

Final remarks

We investigated vibrational spectra of water confined in different types of carbon nanotubes using classical molecular dynamics simulations and quantum mechanical perturbation theory. In these nanopores various types of water structures arise with significant hydrogen bonding networks. In our studies we focused on the OH stretch of HOD in D_2O , because we expected that it should be possible to identify diverse types of water configurations under confinement through their spectroscopic signature.

We started by calculating OH stretch frequencies for single-file water confined in a (6,6) single walled carbon nanotube. The resulting frequency distribution showed very distinct characteristics. It consists of two peaks with different linewidth, representing the bonded and the free state of the hydrogens. This spectrum is very different from its counterpart for bulk, which consists of a single peak.

Subsequently we went on studying water in tubes with diameters larger than 1.09 nm. In this case, water forms cylindrical structures with a very characteristic hydrogen bonding network. We can distinguish two types of OH stretches in these systems. One kind is pointing in the direction of the axis (inter-ring hydrogens), the otherone perpendicular (intra-ring hydrogens) to it. However, the frequency distributions of these water structures showed only one peak, because of the similarity in the next neighbour positions between both kinds of hydrogens. Nevertheless, the infrared spectra of these systems showed two peaks on account of motional narrowing. This effect revealed the distinct hydrogen bond topology. Despite that, these spectra are still very different from their single-file counterpart. The fre-

quency shift between the intra-ring and inter-ring peak is much smaller than that for the free peak and bond peak in single-file water and in contrary to single-file water the linewidths of the peaks are nearly the same.

In a (10,10) CNT we found disordered liquid-like water. Its infrared spectra showed a broad peak featuring a smaller peak attached on the blue side. The latter is caused by a surface effect. Hydrogens pointing in direction of the tube wall cannot find a bonding partner and their OH stretch frequency increases.

All these spectra are very different from each other and therefore our results suggest that it is indeed possible to distinguish between single-file water, cylindrical water, disordered tube water and bulk water through vibrational spectroscopy.

Appendix A

Derivation of the eigenfunctions of the Schrödinger equation for the Morse potential

To obtain the analytical solutions of the Schrödinger equation for the 1D Morse potential we follow a derivation by Boccara [34].

First we introduce the variable $Q = r - r_0$ where r is the spatial coordinate, r_0 is the minimum of the Morse Potential and Q is the distance from it. The Morse potential $V(r)$ is given by:

$$V(r) = d(1 - e^{-aQ})^2. \quad (\text{A.1})$$

Since we neglect coupling of OH oscillations, and we are only interested in time independent properties, we can use the stationary Schrödinger equation in one dimension with the reduced mass $\mu = 1/(\frac{1}{m_O} + \frac{1}{m_H})$ and its n^{th} eigenstates:

$$\left(-\frac{\hbar^2}{2\mu} \frac{d^2}{dr^2} + V(r) \right) \psi_n(r) = E_n \psi_n(r). \quad (\text{A.2})$$

We introduce the variable $u = aQ$ and express the above equation in terms of u :

$$\left(\frac{d^2}{du^2} + \frac{2\mu}{a^2 \hbar^2} (E - V(u)) \right) \psi_n(u) = 0. \quad (\text{A.3})$$

Next, we perform the transformation $x = e^{-u}$. Since we are dealing with a differential equation, we have to transform the derivative du ,

$$dx = -e^{-u} du ,$$

and obtain

$$\left(\frac{d^2}{dx^2} + \frac{1}{x} \frac{1}{dx} + \frac{2\mu}{a^2 \hbar^2} \left(\frac{E}{x^2} + \frac{2D}{x} - D \right) \right) \psi_n(x) = 0 . \quad (\text{A.4})$$

We make an ansatz for the wave functions $\psi_n(x)$, with new variables d and b , which we will define later:

$$\psi_n(x) = e^{-dx} (2dx)^{b/2} F_n(x) . \quad (\text{A.5})$$

Instead of Equ. (A.4), we obtain a differential equation for $F_n(x)$:

$$\begin{aligned} & \frac{2\mu}{a^2 \hbar^2} \left(\frac{E}{x} - D(-2+x) \right) F_n(x) \\ & + \frac{1}{4} \left(\frac{b^2}{x} - 4bd + 4d(-1+dx) \right) F_n(x) \\ & + (1+b-2dx) \frac{d}{dx} F_n(x) + x \frac{d^2}{dx^2} F_n(x) = 0 . \end{aligned} \quad (\text{A.6})$$

We define the newly introduced variables d and b ,

$$\begin{aligned} D &= \frac{\sqrt{\mu d}}{a \hbar} , \\ E &= \frac{-a^2 \hbar^2 b^2}{8\mu} , \end{aligned}$$

and transform Equ. (A.6) to the coordinate $z = 2dx$, to obtain a simplified expression:

$$\left[\left(\frac{2\mu D}{a^2 \hbar^2 d} - \frac{b+1}{2} \right) + (b+1-z) \frac{d}{dz} + z \frac{d^2}{dz^2} \right] F_n(z) = 0 . \quad (\text{A.7})$$

Further, we define:

$$A = \frac{2\mu D}{a^2 \hbar^2 d} ,$$

and recognize Equ. (A.7) as the defining equation for the generalized Laguerre polynomials: $F_n^b(z) = L_{A-(b+1)/2}^b(z)$, where we introduced the discrete eigenstates $n = A - (b+1)/2$.

By inserting the Laguerre polynomials into Equ. (A.5), we obtain the desired eigenfunctions:

$$\psi_n(x) = e^{-dx}(2dx)^{b/2}L_n^b(2dx). \quad (\text{A.8})$$

These are the same wavefunctions as proposed in Equ. (2.13).

Note that the energy levels of the Morse potential are finite, because $L_{A-(b+1)/2}^b(z)$ is only defined for $b > 0$. This implies a restriction on n and limits the number of eigenfunctions:

$$n \leq A - \frac{1}{2}. \quad (\text{A.9})$$

Bibliography

- [1] J. Köfinger, G. Hummer, and C. Dellago. Macroscopically ordered water in nanopores. *Proceedings of the National Academy of Science*, 105:13218–13222, 2008.
- [2] W. Wenseleers, S. Cambre, J. Culin, and A. Bouwen. Effect of Water Filling on the Electronic and Vibrational Resonances of Carbon Nanotubes: Characterizing Tube Opening by Raman Spectroscopy. *Advanced Materials*, 19:9635–9648, 2007.
- [3] S. Cambré, B. Schoeters, S. Luyckx, E. Goovaerts, and W. Wenseleers. Experimental observation of single-file water filling of thin single-wall carbon nanotubes down to chiral index (5,3). *Phys. Rev. Lett.*, 104:207401, 2010.
- [4] J. Köfinger, G. Hummer, and C. Dellago. A one-dimensional dipole lattice model for water in narrow nanopores. *The Journal of Chemical Physics*, 130:154110, 2009.
- [5] Jürgen Köfinger and Christoph Dellago. Orientational dynamics and dielectric response of nanopore water. *Phys. Rev. Lett.*, 103:080601, 2009.
- [6] C. Dellago, M. M. Naor, and G. Hummer. Proton Transport through Water-Filled Carbon Nanotubes. *Phys. Rev. Lett.*, 90:105902, 2003.
- [7] C. Dellago and G. Hummer. Kinetics and Mechanism of Proton Transport across Membrane Nanopores. *Phys. Rev. Lett.*, 97:245901, 2006.
- [8] K. Koga, G. T. Gao, H. Tanaka, and X. C. Zeng. Formation of ordered ice nanotubes inside carbon nanotubes. *Nature*, 412:802–805, 2001.

- [9] D. Takaiwa, I. Hatano, K. Koga, and H. Tanaka. Phase diagram of water in carbon nanotubes. *Proceedings of the National Academy of Sciences*, 105:39–43, 2008.
- [10] K. Nakamoto, M. Margoshes, and R. E. Rundle. Stretching Frequencies as a Function of Distances in Hydrogen Bonds. *Journal of the American Chemical Society*, 77:6480–6486, 1955.
- [11] A. Novak. Hydrogen bonding in solids correlation of spectroscopic and crystallographic data. *Large Molecules*, 18:177–216, 1974.
- [12] J. D. Eaves, A. Tokmakoff, and P. L. Geissler. Electric Field Fluctuations Drive Vibrational Dephasing in Water. *The Journal of Physical Chemistry A*, 109:9424–9436, 2005.
- [13] S. A. Corcelli and J. L. Skinner. Infrared and Raman Line Shapes of Dilute HOD in Liquid H₂O and D₂O from 10 to 90°. *The Journal of Physical Chemistry A*, 109:6154–6165, 2005.
- [14] B. Reischl, J. Köfinger, and C. Dellago. The statistics of electric field fluctuations in liquid water. *Molecular Physics*, 107:495–502, 2009.
- [15] D. Chandler. *Introduction to Modern Statistical Mechanics*. Oxford University Press, 1987.
- [16] H. J. C. Berendsen, J. R. Grigera, and T. P. Straatsma. The missing term in effective pair potentials. *The Journal of Physical Chemistry*, 91:6269–6271, 1987.
- [17] R. Watts. An accurate potential for deformable water molecules. *Chemical Physics*, 26:367–377, 1977.
- [18] J. R. Reimers and R. O. Watts. A local mode potential function for the water molecule. *Molecular Physics*, 52:357–381, 1984.
- [19] I. A. Watson, B. R. Henry, and I. G. Ross. Local mode behavior: The Morse oscillator model. *Spectrochimica Acta Part A: Molecular Spectroscopy*, 37:857–865, 1981.
- [20] E. Schrödinger. Quantisierung als Eigenwertproblem. *Annalen der Physik*, 384:489–527, 1926.

- [21] E Fermi, editor. *Nuclear physics*. University of Chicago Press, 1950.
- [22] P. P. Ewald. Die Berechnung optischer und elektrostatischer Gitterpotentiale. *Annalen der Physik*, 369:253–287, 1921.
- [23] R. Zwanzig. *Nonequilibrium Statistical Mechanics*. Oxford University Press, USA, 2001.
- [24] L. Verlet. Computer Experiments on Classical Fluids. I. Thermodynamical Properties of Lennard-Jones Molecules. *Phys. Rev.*, 159:98, 1967.
- [25] J.-P. Ryckaert, G. Ciccotti, and H. J. C. Berendsen. Numerical integration of the Cartesian equations of motion of a system with constraints: molecular dynamics of n-alkanes. *Journal of Computational Physics*, 23:327–341, 1977.
- [26] G. Hummer. 1D Lattice Sums. unpublished.
- [27] A. Striolo, A. A. Chialvo, K. E. Gubbins, and P. T. Cummings. Water in carbon nanotubes: Adsorption isotherms and thermodynamic properties from molecular simulation. *The Journal of Chemical Physics*, 122:234712, 2005.
- [28] J. D. Smith, R. J. Saykally, and P. L. Geissler. The Effects of Dissolved Halide Anions on Hydrogen Bonding in Liquid Water. *Journal of the American Chemical Society*, 129:13847–13856, 2007.
- [29] F. Paesani, S. S. Xantheas, and G. A. Voth. Infrared Spectroscopy and Hydrogen-Bond Dynamics of Liquid Water from Centroid Molecular Dynamics with an Ab Initio-Based Force Field. *The Journal of Physical Chemistry B*, 113:13118–13130, 2009.
- [30] J. J. Loparo, C. J. Fecko, J. D. Eaves, S. T. Roberts, and A. Tokmakoff. Reorientational and configurational fluctuations in water observed on molecular length scales. *Phys. Rev. B*, 70:180201, 2004.
- [31] C. J. Fecko, J. J. Loparo, S. T. Roberts, and A. Tokmakoff. Local hydrogen bonding dynamics and collective reorganization in water: Ul-

- trafast infrared spectroscopy of HOD/D₂O. *The Journal of Chemical Physics*, 122:054506, 2005.
- [32] G. S. Fanourgakis and S. S. Xantheas. Development of transferable interaction potentials for water. V. Extension of the flexible, polarizable, Thole-type model potential (TTM3-F, v. 3.0) to describe the vibrational spectra of water clusters and liquid water. *Journal of Chemical Physics*, 128, 2008.
- [33] O. Byl, J.-C. Liu, Y. Wang, W.-L. Yim, J. K. Johnson, and J. T. Yates. Unusual Hydrogen Bonding in Water-Filled Carbon Nanotubes. *Journal of the American Chemical Society*, 128:12090–12097, 2006.
- [34] N. Boccara. *Essentials of Mathematica: With Applications to Mathematics and Physics*. Springer-Verlag New York, 2007.

Marcus Weinwurm

PERSONAL DETAILS

- Name: Marcus Weinwurm
- Nationality: Austrian
- Birth date: 15.01.1985
- Address: Mayerhofgasse 3/W, A-1040 Wien
- E-mail: marcus.weinwurm@gmx.net

EDUCATION

- **Study of Physics, University of Vienna**
 - October 2005 - June 2010 (expected date of graduation)
 - *Diploma thesis in Statistical Physics*: calculating infrared and Raman spectra of confined water in different carbon nanotubes, supervised by Univ.-Prof. Mag. Dr. Christoph Dellago
 - *Practical course in Computational Physics*: studying the phase diagram of the Gaussian core model for polymers by use of molecular dynamics software for graphic cards, supervised by Univ.-Prof. Dr. Martin Neumann
 - *Practical course in Quantum Optics*: checking the Bell inequalities, building an HeNe laser, and measuring the Lamp-dip through saturated spectroscopy, supervised by Univ.-Prof. Dr. Markus Arndt
- **Secondary schools**
 - 2000 - 2004 Commercial High School Schärding am Inn, Austria
 - 1999 - 2000 Commercial High School Ried im Innkreis, Austria
- **Primary schools**
 - 1995 - 1999 Hauptschule St. Martin im Innkreis, Austria
 - 1991 - 1995 Volksschule Ort im Innkreis, Austria

WORK EXPERIENCE

- **Tutor**, Introduction into Mathematical Methods for Physicists I, University of Vienna, October - December 2009
- **Tennis instructor** at the TC Ort-Antiesenhofen, Summer 2008/09

SKILLS

- **Electronic Data Processing**
Programming languages: C/C++, Fortran, Shell script, Latex, VB
Operating systems: Linux and Windows releases
Software proficiency: Wolfram Mathematica, Matlab, HOOMD, OriginLab, Adobe Premiere, Office suites
- **Languages**
German: native speaker
English: fluent
French: basic writing

OTHER ACTIVITIES

- Civilian Service, Lebenshilfe Ried, October 2004 - September 2005
- Competing in multiple tennis championships for the TC Ort-Antiesenhofen
- Private study of Philosophy